SELF-HEALING OF DELAMINATION DAMAGE IN GLASS/EPOXY COMPOSITES USING CATALYST FUNCTIONALIZED FIBERS

BY

KEVIN RICHARD HART

THESIS

Submitted in partial fulfillment of the requirements
for the degree of Master of Science in Aerospace Engineering
in the Graduate College of the
University of Illinois at Urbana-Champaign, 2012

Urbana, Illinois

Adviser:

Professor Scott White

ABSTRACT

The use of polymer matrix fiber-reinforced composites in structural applications is growing because of the excellent specific strength and stiffness of these materials. Their wide spread acceptance, however, has been limited in some areas because of susceptibility to damage from impact events in directions transverse to the direction of fiber reinforcement. Damage occurring from transverse impact events is multi-dimensional, difficult to predict and visually difficult to detect. This complexity leads to more expensive maintenance, which in many cases offsets the original benefits of these lightweight materials. As an alternative, self-healing polymers have been introduced as a way to autonomically repair damage in fiber-reinforced polymer composites, ultimately reducing maintenance costs associated with their use.

In this work, self-healing applications are explored in 2D woven glass/epoxy composites for ultimate use in 3D woven composites. Initial work focuses on a new method for introducing self-healing components into low temperature cure 2D fiber-reinforced polymer composites. In these studies, glass fiber preforms are functionalized with second generation Grubbs' catalyst using an evaporative crystallization technique for catalyst deposition. Preforms are then used in the manufacture of laminated 2D woven composites. Healing of interlaminar fracture damage is evaluated in these composites using double cantilever beam (DCB) specimens. Recovery of interlaminar fracture damage is initiated by the injection of liquid dicyclopentadiene (DCPD) onto the fracture surface of the functionalized fiber composites whereby the catalyst on the surface of the fibers triggers a ring opening metathesis polymerization (ROMP) reaction in the liquid monomer, healing the interlaminar damage. Recovery of up to 10% of critical strain energy release rates is observed. Minimal recovery is attributed, in part, to weak bonding between the polymerized DCPD and the surrounding materials. Tortuous crack paths limit interfacial fiber/matrix de-bond required to expose the catalyst coated fiber surface and also introduce crack blunting mechanisms that increase virgin critical strain energy release rates.

In later work, optimization of the fiber functionalization technique is extended to high temperature cure glass/epoxy composites. Alternate methods for catalyst functionalization are examined and dip coating techniques are shown to more evenly and consistently deposit the catalyst on the fiber surface. Thermal and chemical stability of the second generation Grubbs'

catalyst is verified using pure polymer bullet samples. Optimization of fiber architectures is carried out and an 8-harness satin weave is chosen as the optimal system based on double cantilever beam testing. This fabric exhibited more stable crack propagation and greater interfacial fiber/matrix failure and fiber bridging during testing. Small model DCB specimens are used to qualitatively assess healing potential and results indicate that a high catalyst loading is required to demonstrate healing in high temperature cure glass/epoxy composites.

TABLE OF CONTENTS

CHAPTER 1: INTRODUCTION

1.1 Introduction

Fiber-reinforced composites are garnering increased attention in a wide range of industries because of their superior specific in-plane properties. However, complexities of the damage modes associated with composite failure have limited their wide spread acceptance in many areas. Since most manufacturing techniques involve compiling many individual lamina to create a composite laminate, these materials often lack significant load bearing capability in directions perpendicular to the laminated plane. This orthotropic behavior leads to a structure which is especially prone to damage from out-of-plane loading and impact events.

Damage in composites occurring from low velocity, out-of-plane impact events is usually sub-surface, difficult to visually detect, and significantly reduces the stiffness and strength of the structure. In applications where it is desirable to maintain the original structure, non-destructive evaluation methods are required to inspect the damaged regions. These methods are time consuming, require access to damaged parts, require operators with expertise, require complex tools to perform and are expensive. Even when damage from impact events has been detected, it is difficult to repair. Repair techniques often depend upon patches to the composite architecture or resin infiltration of the damaged zone, and rarely do these techniques fully recover the original properties of the material.

Self-healing polymers offer a way to combat expensive detection and repair techniques. These materials utilize a damage triggering mechanism to initiate a healing response, eliminating the costs of manual intervention. Self-healing polymers were pioneered in 2001 by White *et al* [1] using a system based on the ring opening metathesis polymerization (ROMP) of dicyclopentadiene using a Grubbs' catalyst initiator. Since that time, the field has grown substantially and many new systems have been examined. A recent review of self-healing materials is provided by Blaiszik *et al* [2]. Extension of the first generation Grubbs' catalyst and DCPD monomer microencapsulated self-healing system has been used to demonstrate self-repair of impact damage in 2D woven polymer composites by Patel *et al* [3]. However,

extensions of this healing chemistry to 3D woven composites have proven difficult because of a heterogeneous distribution of self-healing components in the final composite. In this thesis, alternate methods of incorporating healing components into 2D woven composites are evaluated.

1.2 Composite Fabric Architecture

Fiber-reinforced composites are often classified by their fiber architecture. To increase the global load bearing capabilities of composites, it is desired to keep fibers straight in their final form to avoid complications in load transfer and keep fiber volume fractions high. Also, curved or bent fibers lead to more complicated damage mechanisms such as micro-buckling and kinking [4–7]. As such, fiber tows in composites with continuous reinforcement tend to run in a single direction. This limitation leads to a classification scheme in which fabric architecture is described by the dimensions (either 1D, 2D or 3D) in which the continuous reinforcement travels.

Unidirectional (1D) composites contain fibers which run continuously in only one direction. High fiber volume fractions can be achieved in unidirectional composites, since the geometry of the reinforcement is much less tortuous and allows fibers to better settle during manufacture. Unidirectional composites carry large loads in directions parallel to the fibers, but are very weak in directions perpendicular to the fibers. Therefore, to increase strength and stiffness in directions perpendicular to fiber travel, two-dimensional (2D) architectures are typically used.

Two-dimensional (2D) architectures are fabricated in a variety of ways. Two common methods involve either stacking unidirectional layers or weaving fibers together in a planar fashion before matrix infusion. Woven layers can also be laminated to create a multi-layer 2D woven structure (Fig 1.1-a). Both methods yield a product in which fibers run continuously in planar directions, but lack through thickness reinforcement. As previously mentioned, these materials provide excellent in-plane properties, but are prone to damage from out-of-plane loading events because of the lack of load bearing capabilities in the out-of-plane direction.

While methods for weaving two-dimensional glass fiber reinforcements are well established, methods for creating 3D woven architectures are much less common. There are

several techniques for creating 3D reinforcement such as weaving, stitching, braiding, and knitting, however, the manufacturing processes are often complex. Recently, however, Mohamed *et al* [8] have patented a weaving process in which a two-dimensional architecture is held together by a binding z-tow creating a preform where reinforcement is arranged orthogonally in all three principal directions (Fig. 1.1-b). It is hypothesized that through thickness reinforcement improves damage resistance through crack pinning, delamination deflection, and improved through-thickness load carrying capabilities.

This thesis will target self-healing applications of 3D composites but will use 2D architectures as a platform to demonstrate feasibility. Damage in 2D woven composites can be more accurately controlled and is more suitable for evaluations of experimental self-healing systems.

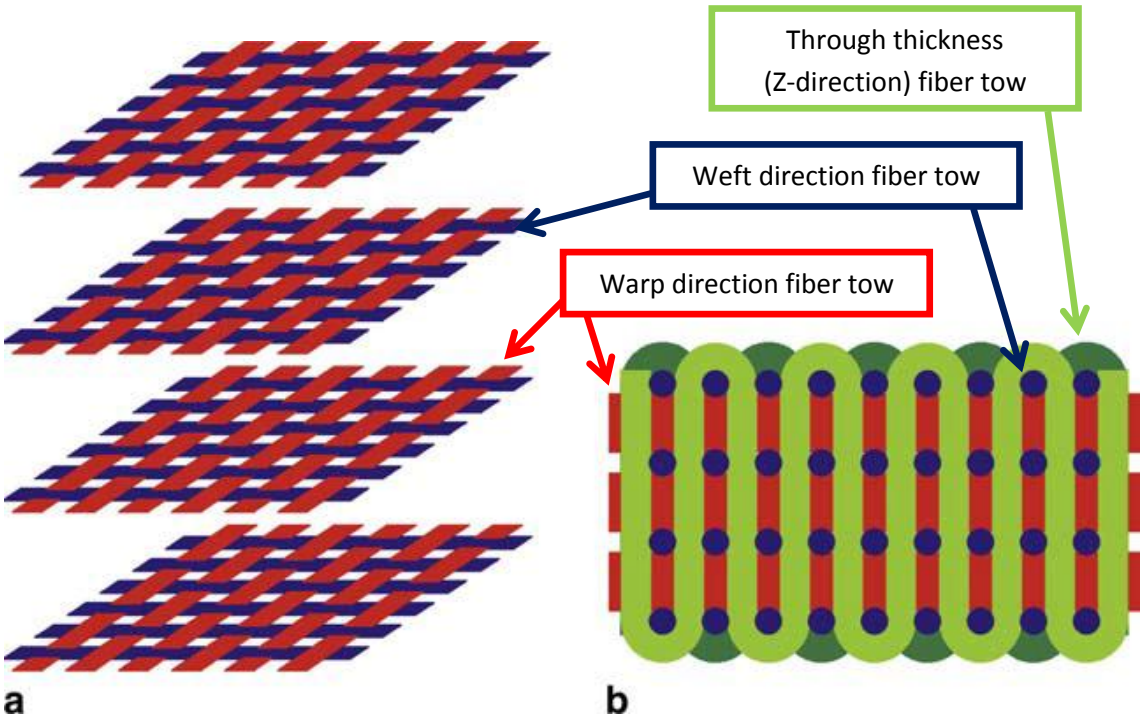

Figure 1.1. Architectural schematics of (a) a stack of 2D plain woven preforms and (b) a 3D orthogonal woven preform (reprinted from Baucom et al. [19] with permission from Elsevier).

1.3 Impact Damage in 2D and 3D Woven Composites

Impact damage in 2D and 3D woven composites weaken global properties by introducing delaminations between ply layers, intra-ply transverse cracks, fiber de-bond, and, in extreme cases, fiber rupture. Delaminations are especially threatening, because they significantly reduce critical buckling loads, reduce residual compressive strength and grow in response to fatigue loading [9–19].

In creating a self-healing composite system, understanding damage mechanisms is important. Previous studies have shown that healing efficiencies of polymer systems is directly related to the volume of damage which is filled by self-healing components [3, 20]. Patel *et al* [21] have used cross-sectional fractography in combination with optical microscopy to investigate delamination separations in 2D plain woven and 3D orthogonal woven glass/epoxy composites. These studies have shown that at the same impact energy, delamination length and separation is reduced in composites with 3D architectures, mainly due to delamination deflection from the through thickness z-tows. Baucom *et al* [18, 19] investigated the response of multiple impact events on 2D and 3D woven composites and concluded that material damage in 3D systems was dissipated over larger areas when compared to 2D woven systems, reducing delamination separations. Optical images from Patel *et al* [21] also reveal the complex damage mechanisms that are present in 2D and 3D composites. Delaminations, transverse matrix cracking and interfacial fiber/matrix failure are present in both systems (Fig. 1.2). To fully recover mechanical properties in these composites, the healing of multiple failure modes is required.

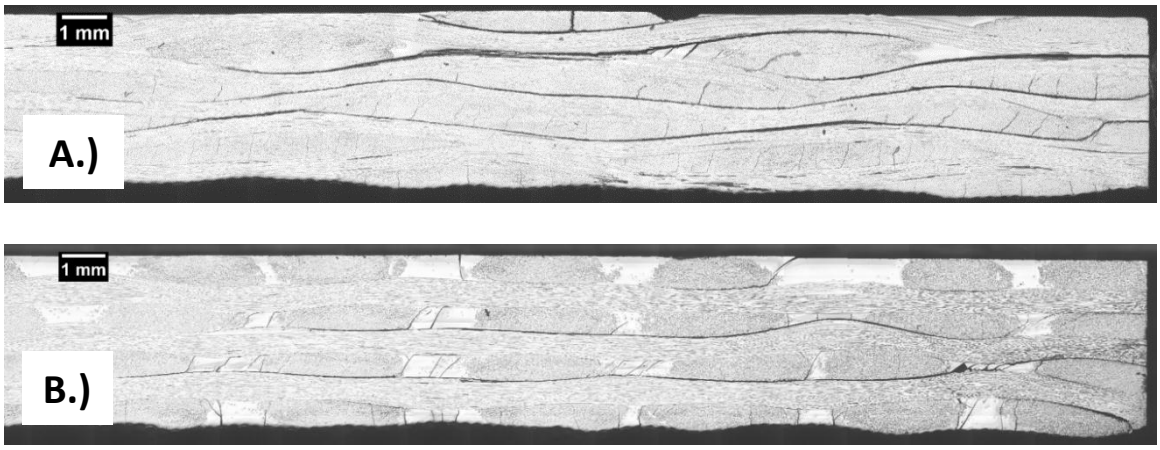

Figure 1.2. Cross sectional images of impacted A.) 2D plain woven and B.) 3D orthogonal woven composites. Images from PhD thesis of AJ Patel [21].

1.4 Self-Healing Materials

While many self-healing systems have been investigated, their application to impact damage in fiber-reinforced composites is limited. Damage volumes can vary drastically depending on reinforcement architecture, constituent properties and impact damage mechanisms. Crack separations ranging from microns to millimeters have been observed in the literature [3, 18, 19, 21]. Therefore, the healing system chosen must sufficiently fill the damage – large or small - which has been introduced.

Microcapsule based systems have received a great deal of attention as a healing mechanism in fiber-reinforced composites. The original Grubbs'/DCPD system reported by White *et al* [1] was extended to fiber-reinforced composites by multiple authors. Kessler *et al* [22] demonstrated self-activated healing in a laminated woven glass/epoxy composite using double cantilever beam (DCB) specimens to simulate delaminations - demonstrating healing efficiencies of up to 19%. Kessler *et al* [23] also fabricated a self-healing graphite/epoxy system using encapsulated DCPD monomer and embedded first generation Grubbs' catalyst – demonstrating average healing efficiencies of up to 66% with the addition of heat during the curing cycle. Patel *et al* [3] investigated autonomic healing of low velocity impact damage in 2D woven glass/epoxy composites using embedded wax protected Grubbs' catalyst microspheres

and DCPD capsules between ply layers. At some impact energies, up to 100% recovery of virgin compressive strength was observed, however at higher impact energies healing efficiencies are reduced to zero due to a large damage volume.

1.5 Extension of Self-Healing 2D Composites to 3D

Patel *et al* [21] have made attempts at incorporating self-healing components into 3D composites to show recovery of impact damage. In this work, Grubbs'-in-wax microspheres and DCPD monomer microcapsules were impregnated into a 3D composite preform using an aqueous suspension. After composite fabrication, samples were impacted and tested in four point bend to evaluate maximum global stress in a flexure after impact (FAI) protocol. Minimal recovery in global maximum strength was observed in the self-healing specimens.

Cross sections of impacted self-healing specimens show a heterogeneous distribution of capsules, localized in the resin-rich regions of the composite (Fig. 1.3). This heterogeneity leads to healed delaminations in resin-rich regions of the composite where capsules agglomerate; large delaminations between tows, however, are unhealed. Insufficient polymerization distance was confirmed by studies of the propagation distance of healed DCPD from ruptured catalyst sites. Additionally, lap shear testing demonstrated that the adhesive strength of polymerized DCPD (pDCPD) to the surrounding epoxy matrix was an order of magnitude lower than the adhesive strength of the epoxy matrix to itself, indicating that poor adhesion also limits healing.

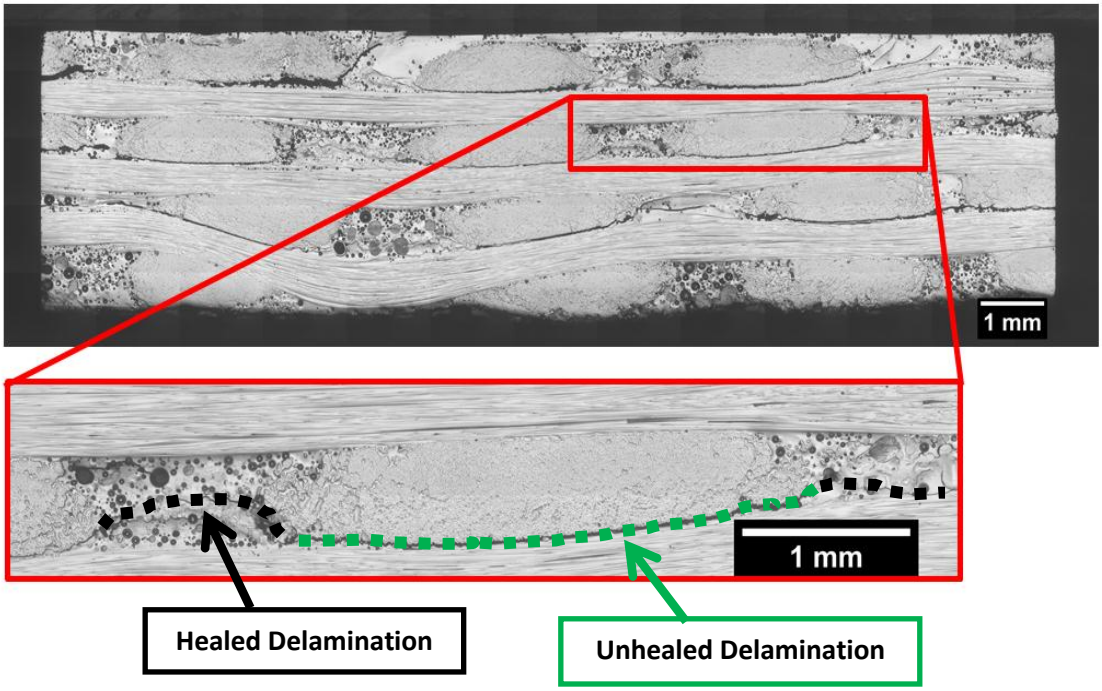

Figure 1.3. Cross section of 3D orthogonal woven composite containing DCPD microcapsules and first generation Grubbs'-in-wax microspheres after an impact triggered healing event. A heterogeneous distribution of healing components leads to unhealed delaminations in tow overlap regions.

1.6 Objective of Current Work

This thesis focuses on an alternate approach to incorporating self-healing components into 2D and 3D orthogonal glass/epoxy composites for post-impact recovery of mechanical properties. In chapter 2, catalyst functionalization of glass fiber preforms is explored as an approach to achieve a more homogeneous distribution of catalyst through the composite. 2D woven composites are utilized as a test bed for evaluating healing by measuring mode I critical strain energy release rates of virgin and self-activated double cantilever beam (DCB) composite specimens.

In chapter 3, fiber functionalization is evaluated for use in high temperature cure glass/epoxy composites. Catalyst functionalization methods are examined. Thermal and chemical stability of first and second generation Grubbs' catalyst in the presence of high temperature cured epoxy systems is discussed. Optimization of fiber architecture is carried out to determine maximum healing efficiencies capable with the fiber functionalized healing system.

Chapter 4 discusses limitations of the Grubbs'/DCPD healing chemistry and offers potential future directions for self-healing 3D composites. An alternate microcapsule based healing system using epoxy and amine microcapsules is discussed. Methods of introducing microvascular networks into 3D composites for self-healing applications are also presented.

CHAPTER 2: SELF-ACTIVATED 2D WOVEN COMPOSITES WITH CATALYST FUNCTIONALIZED FIBERS

2.1 Introduction

Autonomic repair of impact damage in 3D woven composites containing Grubbs'-in-wax microspheres and DCPD monomer capsules subject to out-of-plane impact is hindered by delaminations which span fiber tow overlap regions. Because of processing techniques, capsules agglomerate in resin-rich regions of the composite leaving tow overlap regions devoid of catalyst and monomer capsules, hindering recovery. Observations of a damaged 3D composite cross section (Fig. 1.2-b) show that interfacial de-bond is particularly prominent in tow overlap regions of the 3D woven composites. This chapter explores the possibility of functionalizing glass fibers with Grubbs' catalyst to provide catalyst in areas of interfacial fiber/matrix de-bond in a damaged composite, facilitating ROMP in those regions.

Fiber functionalization has been explored in the past as an avenue for catalyst delivery. Blaiszik *et al* [24] used first generation Grubbs' catalyst functionalized single glass fibers in a model composite system with ca. 1.5 μm DCPD capsules to demonstrate recovery of interfacial shear strength in single fiber pull out tests. In these studies, a dip coating technique employing a solution of catalyst dissolved in benzene was utilized for catalyst deposition. Recovery of interfacial shear strength of up to 40% was observed using single fiber pull out tests, but virgin properties were reduced with the introduction of capsules. Sanada *et al* [25] investigated self-healing potential of transverse cracks in unidirectional graphite/epoxy tensile specimens in which the fibers were coated in an epoxy/catalyst/capsule mixture before solidification. However only minor levels of healing were achieved and capsule loading was as high as 40 wt%, reducing the virgin properties significantly. In both of these studies, limited recovery of mechanical properties was observed. Limited recovery in epoxy systems containing first generation Grubbs' catalyst has been attributed to the chemical incompatibility of the catalyst with amines often present in co-curing agents. Brown *et al* [26] reported complete deactivation of the first generation catalyst when directly mixed with the co-curing agent Diethylenetriamine (DETA) before epoxy polymerization. Chemical deactivation of the first generation catalyst in the presence of reactive amine groups is described in detail by Wilson *et al* [27]. However,

Brown *et al* [26] demonstrated that with catalyst particle sizes large enough, the catalyst protects itself from complete deactivation in epoxy systems.

While the first generation catalyst is relatively unstable and quick to deactivate in the presence of amine groups, the second generation catalyst demonstrates a much more complex behavior. Wilson *et al* [28] report on the creation of new novel carbene complexes capable of ROMP when the second generation catalyst is added to various amines. Increased thermal and chemical stability is also reported. Wilson *et al* [27] also report higher healing efficiencies in ROMP systems initiated by the second generation catalyst; the addition of heat during this process increasing the healing efficiency even further.

In this chapter, full-scale catalyst functionalized fiber composites are investigated as a new method for incorporating Grubbs' catalyst into self-healing composites. Glass fiber preforms are functionalized with second generation Grubbs' catalyst using a super-saturated evaporative crystallization technique for catalyst deposition. Preforms are then used in the manufacture of 2D woven composites. Healing of interlaminar fracture damage is evaluated using double cantilever beam (DCB) specimens. Reference tests using pre-catalyzed monomer and pre-mixed epoxy as the healing agent are compared with self-activated healing results.

2.2 Materials and Methods

2.2.1 Fiber Functionalization and Self-Healing Materials

To most accurately mimic the 3D fabric architecture described in section 1.2, 2D woven preforms with similar properties were chosen. For this study, 24 oz/yd^2, 5 x 5 yarns/inch plain woven S2-glass fabric preforms (Owens Corning Knytex SBA240F) were selected. Fiber functionalization was achieved using a solution of second generation Grubbs' catalyst (Sigma-Aldrich) dissolved in Benzene (Alfa-Aesar). Second generation Grubbs' catalyst was obtained as a solid brown powder and used as received. Gaseous nitrogen was bubbled through as received liquid benzene (Alfa-Aesar) for a minimum of 10 minutes before use to remove excess moisture. Solid catalyst (0.5 g) was slowly added to the solvent (49.5 g) to create a 1 wt% solution. Upon the addition of the catalyst, the solution instantly turned a light red color and no catalyst crystals were observed in solution, indicating full dissolution. The solution was allowed to mix for a minimum of 5 minutes on a mixing plate before use.

To functionalize the fabric, preforms were cut to 248 mm x 248 mm and placed into a 254 mm x 254 mm aluminum pan. The solution containing catalyst and benzene was then poured over the fabric. The fabric was agitated and flipped one time then left uninterrupted for 24 hours in a fume hood at room temperature to allow for complete benzene evaporation. Final functionalized preforms were a deep red color, indicating catalyst deposition on the surface of the fibers (Fig. 2.1). Mass change of the preforms was approximately 1.0%. To ensure the solvent does not disturb the fabric sizing, non-functionalized control specimens using a solution of only benzene were fabricated in the same manner. After evaporation of the benzene, no mass change was observed for these preforms.

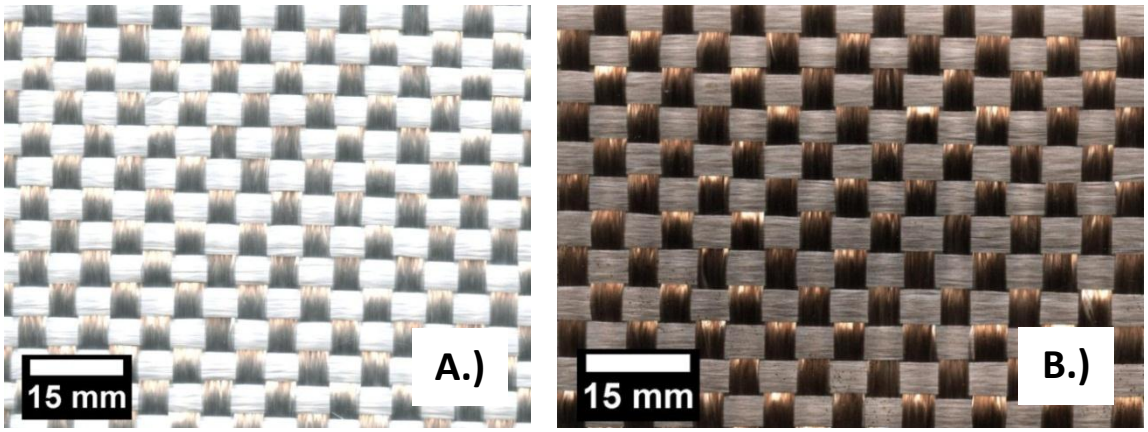

Figure 2.1. Plain (A) and catalyst functionalized (B) plain weave glass fiber preforms.

Freeze dried first and second generation Grubbs' catalyst (Sigma-Aldrich) for pre-catalyzed reference tests were synthesized following the procedure outlined by Jones *et al* [29]. Endo-dicyclopentadiene monomer (Acros Organics) used in self-activated specimens was distilled before use to remove water and other stabilizers using a distillation apparatus at 70 °C under vacuum at 25 torr.

2.2.2 Composite Fabrication

Composite panels were fabricated using 248mm x 248mm glass fiber preforms in a wet hand lay-up procedure. All samples contained 4 woven layers of glass fabric. The epoxy resin matrix was prepared by mixing Araldite LY 8604 resin with Aradur 8604 curing agent (Huntsman Mfg.)

at a ratio of 100:15, respectively. Once mixed, the epoxy was degassed for a minimum of 20 minutes under vacuum before use. Four cups of epoxy were individually mixed, one for each layer of glass fabric.

Once prepared, the first portion of epoxy resin was poured onto the tooling surface of an aluminum plate. A square rubber mold 254 mm x 254 mm was used to contain excess epoxy. Once the tooling surface was adequately coated, a glass fabric layer was lightly placed on the liquid resin with minimal external pressure applied. After approximately ten minutes, full wetting of the fabric was observed. The process was then repeated for the remaining layers. A 248 mm x 102 mm x 25 µm non-porous release film was placed near the mold edge between layers 2 and 3 to provide a pre-crack region for the DCB specimens. Plain specimens contained no functionalized fiber layers. Self-activated specimens contained catalyst functionalized preforms in layers 2 and 3 of the composite lay-up (Fig 2.2). Porous peel ply and bleeder cloth were placed over the lay-up to facilitate resin flow in the transverse direction during the curing process. Composites were cured under 172 kPa of compaction pressure at 35 °C for 24 hours yielding panels approximately 3.25 mm thick. Fiber volume fractions for plain and self-activated specimens were 41% and 42%, respectively, as calculated using a matrix burn-off method.

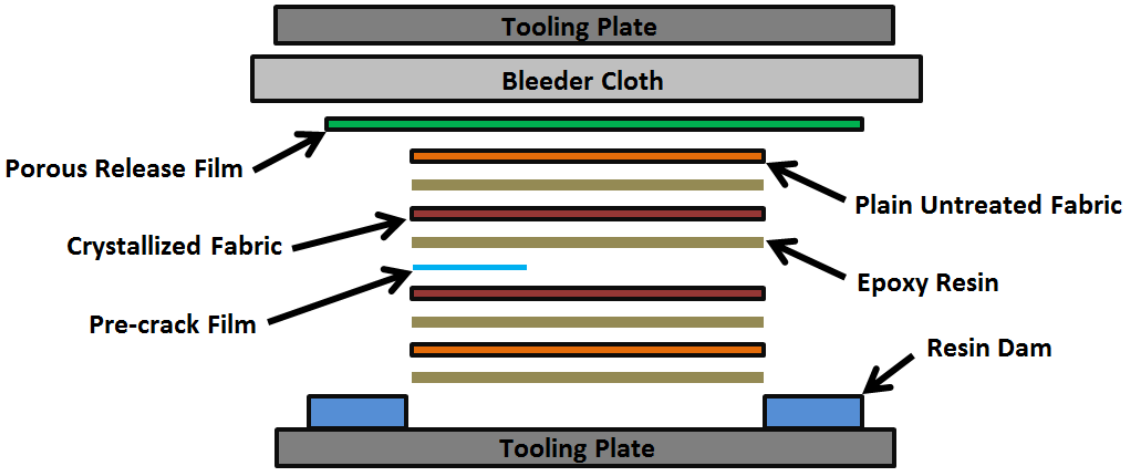

Figure 2.2. Lay-up sequence for fiber functionalized composite specimens.

2.2.3 DCB Specimen Preparation

Following composite manufacture, DCB specimens were cut to size according to ASTM D5528 using a water-jet cooled diamond saw (Fig. 2.3). Piano hinges with a leaf height of 25 mm and an opening distance of 25 mm (National Mfg.) were bonded to the samples using 3M DP-460 High Strength Epoxy. One sample edge was coated with a thin layer of white opaque fluid to aid in visualization of the crack tip during testing. Vertical demarcations were placed along the whitewashed sample edge in 5 mm increments using a fine tip marker to provide a reference for crack length measurements (Fig. 2.4). Demarcations emanated from the end of the pre-crack region and were repeated along the entire crack propagation length.

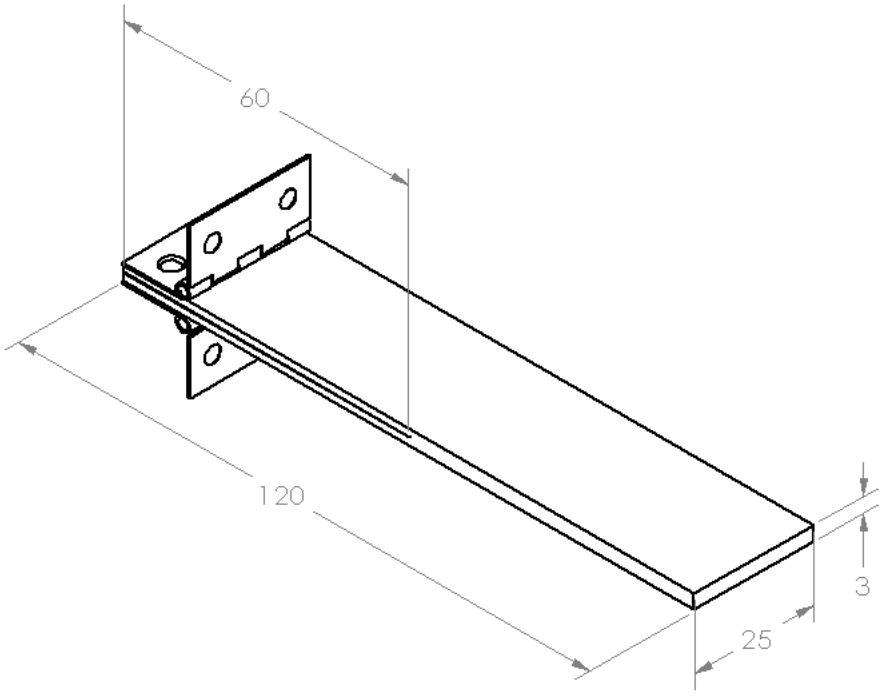

Figure 2.3. Double cantilever beam specimen. All dimensions are in mm.

Figure 2.4. A plain double cantilever beam specimen with 5 mm demarcations.
Darker marks indicate 20 mm segments.

2.3 Testing and Characterization

2.3.1 Testing Procedure

Specimens were tested on a Parker 081-6079 load frame with a Futek LSB300 50 lb. load cell in displacement control at a rate of 5 mm min^{-1} according to ASTM D5528 [30]. A Basler A631fc CCD camera with an affixed Kowa LM16HC zoom lens was mounted on an optical table beside the sample during testing to track the crack during testing. Load and displacement data was taken at a frequency of 100 Hz and images were recorded at every 200 data points (0.5 Hz). Images were synced with load/displacement data using LABVIEW software.

During virgin sample tests, specimens were loaded to complete failure. Following virgin tests, a variety of reference tests were performed. In all reference tests, the healing agent was injected evenly onto the crack plane using a microliter syringe. Reference tests for plain samples included first generation and second generation pre-catalyzed DCPD monomer injections. In these tests, 1.0 wt% of freeze dried catalyst was pre-mixed with DCPD monomer and reacted for 30 seconds before injection. Epoxy reference samples used Araldite LY 8604 / Aradur 8604 as the healing agents. In fiber functionalized specimens, self-activated samples were evaluated by injecting DCPD monomer directly onto the crack plane. All samples were lightly clamped using binder clips during the cure cycle. Table 2.1 provides a complete list of all tested samples and healing conditions.

Fiber Surface	Functionalization	Samples	Reference Test Type	Samples	Cure Conditions
Plain	None	15	First Generation Pre-catalyzed	3	24 Hours @ 22°C
			Second Generation Pre-Catalyzed	4	24 Hours @ 22°C
			Epoxy Reference	4	4 Days @ 22°C
			Epoxy Reference	4	4 Days @ 22°C
Functionalized	1 wt% 2G Grubbs'	7	Self-Activated	3	24 Hours @ 22°C
			Self-Activated	4	24 Hours @ 22°C
	Benzene Only	7		N/A	

Table 2.1. Summary of DCB results

2.3.2 Data Reduction

Interlaminar, mode I fracture toughness in DCB specimens is recorded using critical strain energy release rate, G_{1C}. If a material is assumed linear elastic, mode I energy release rate in terms of sample compliance for displacement control is expressed as:

$$G_1 = -\frac{1}{b}\frac{\partial \Pi}{\partial a} = \frac{P^2}{2b}\frac{dC}{da} \tag{2.1}$$

where Π is the potential energy of the specimen, a the crack length, b the width, P the load, and C the sample compliance, often taken as the cross-head displacement over the load (δ/P).

In DCB specimens each arm of the specimen is treated as a cantilever beam. This allows for an explicit compliance to be calculated from Euler-Bernoulli beam theory and inserted into Eq. 2.1, yielding the equation:

$$G_1 = \frac{3P\delta}{2ba} \tag{2.2}$$

In practice, however, this equation over predicts values of critical strain energy release rate because it neglects contributions from shear deformation in the specimen arms and rotation which may occur at the cantilevered end [31]. To account for these effects, a

correction factor, Δ, is added to the crack length in Eq. (2.2) to create an effective crack length, $a + |\Delta|$. This correction factor is determined by plotting the cube root of specimen compliance (δ/P) versus unaltered crack length, a. A linear fit is interpolated back to zero compliance, and the offset from zero crack length is recorded as the correction factor as shown in Fig. 2.5. The analysis method is commonly referred to as the modified beam theory (MBT) method.

Self-healing assessments between virgin and healed specimens can be made by comparing critical strain energy release rates:

$$\eta = \frac{G_{1C}^{Healed}}{G_{1C}^{Virgin}} \tag{2.3}$$

where η is the healing efficiency of the strain energy release rates, and G_{1C}^{Healed} and G_{1C}^{Virgin} refer to critical strain energy release rates of healed and virgin specimens.

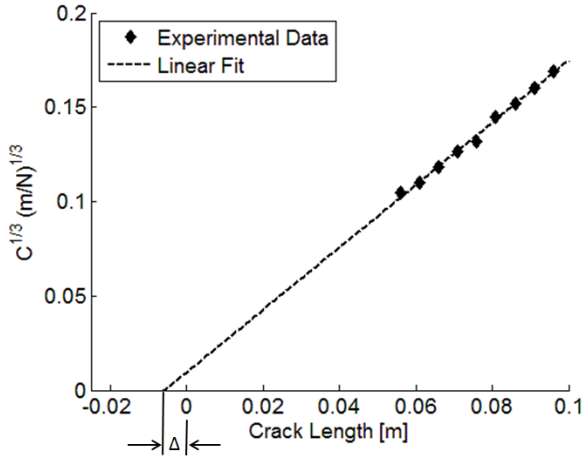

Figure 2.5. Typical cube root specimen compliance plotted against crack length for self-activated specimens. Crack length correction term, Δ, is used in the calculation of critical strain energy release rate using the modified beam theory method.

2.4 Results and Discussion

2.4.1 Virgin Specimens

A typical load-displacement curve for plain specimens is shown in Fig. 2.6. The curve is linear up to a peak load of approximately 34 N at which point a large jump in the load is observed. This is

due to unstable crack propagation in the composite specimen. This continues throughout the duration of the test, resulting in a saw-tooth pattern in the load-displacement data. This type of crack propagation is referred to as stick-slip behavior and has previously been observed in woven composite specimens [22, 32].

Stick slip-behavior in many composite specimens is attributed to the tortuousity of the crack path. In DCB tests, failure is commonly observed to follow the contour of the fabric in the crack plane. In composites containing unidirectional fabric architectures tortuosity is limited since the crack path is relatively well defined. However, in woven specimens much more tortuousity is encountered because of the increased fiber undulations. Since the fabric used in this study is a plain weave and relatively coarse, a great deal of crack pinning and blunting occurs from the architecture.

Critical strain energy release rates were calculated at each one of these dynamic crack propagation sites using Eq. 2.2 with the peak load at fracture, the displacement at peak load, and the crack length immediately before dynamic fracture. A plot of G_{1C} versus crack length shows the Resistance curve (R-curve) behavior in the plain specimens (Fig. 2.7). In many composite specimens, fiber bridging mechanisms often lead to R-curves which exhibit an increasing critical strain energy release rate with increasing crack length. This phenomena is not observed as prominently with this particular composite system. It is hypothesized that the toughening induced from crack pinning due to the tortuous fabric architecture overwhelms any effects caused by the toughening induced from any fiber bridging mechanisms, limiting the usual plateau effect in the R-curve often exhibited by fiber-reinforced composites.

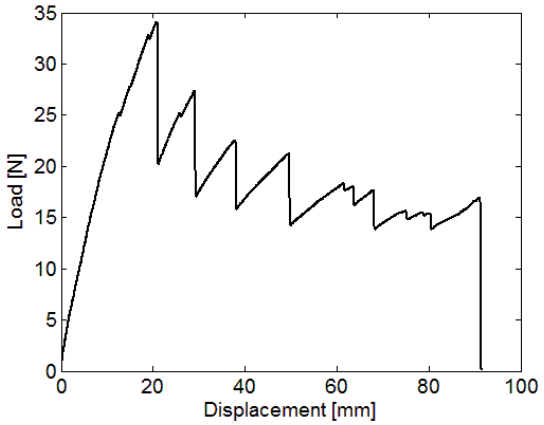

Figure 2.6. A typical virgin load-displacement curve for plain DCB specimens. Plain specimens contain no functionalized fiber layers.

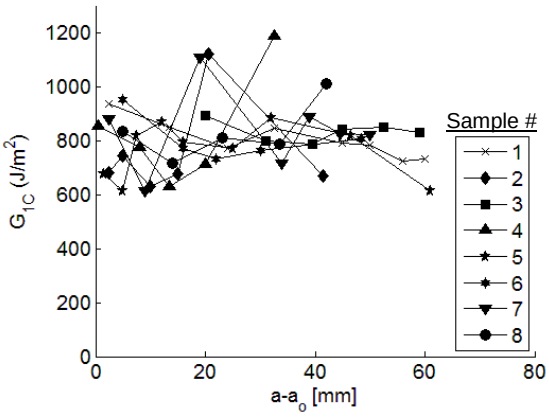

Figure 2.7. Typical R-curves for virgin testing of plain DCB specimens. Plain specimens contain no functionalized fiber layers.

Fiber functionalized samples exhibit a similar stick-slip failure behavior. R-curve behavior for these samples (Fig. 2.8) reveal a slightly higher critical strain energy release rate then plain samples, enumerate less dynamic failure events and display an increase in dynamic crack propagation distance when compared to plain specimens - possibly due to increased crack blunting from the catalyst presence. Further investigation into the role of catalyst functionalization on the strain energy release rate will be carried out in future work.

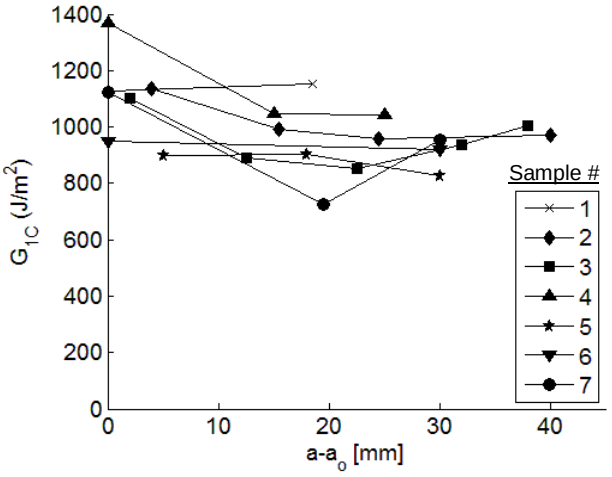

Figure 2.8. Typical R-curves for virgin testing of self-activated reference DCB specimens.

2.4.2 Self-Activated and Reference Specimens

Typical load-displacement data for healed self-activated specimens is plotted alongside virgin specimens in Fig. 2.9-A. The behavior of the crack propagation in the healed specimen is much more stable than that of the virgin samples. This allows the modified beam theory method to be utilized for calculations of critical strain energy release rate, G_{1C} (Eq. 2.3). Two volumes of DCPD monomer were injected into the crack plane following the virgin tests. Samples with 200 µL of monomer delivered showed higher healing values than samples using 500 µL. Previous studies using pure polymer systems have shown that a lower catalyst to monomer ratio decreases overall healing efficiency as catalyst mobility becomes hindered [26]. Optimization of delivered monomer is left for future work. The highest levels of recovery of critical strain energy release rates observed in self-activated specimens is approximately 10%.

Pre-catalyzed samples represent the optimal healing which can be expected for this type of healing system since the catalyst and monomer are pre-mixed before injection into the crack plane. Pre-catalyzed first and second generation studies were conducted. A typical load-displacement curve for pre-catalyzed reference specimens using both first and second generation catalyst are provided in Fig. 2.9-B and 2.9-C, respectively. Again, stable crack propagation is observed in these specimens. Recovery of critical strain energy release rates for the first and second generation pre-catalyzed specimens is 13% and 30% respectively. Neither

system shows full recovery, most likely due to poor bonding which exists between the pDCPD and exposed glass fibers.

Epoxy reference samples represent an optimal healing chemistry for this system. Using the matrix material as a healing agent provides increased mechanisms for chemical bonding between the damaged and healed material. Again, varying amounts of healing agent were delivered. Up to 95% recovery of critical strain energy release rate was observed in the best case for epoxy reference samples. Typical load-displacement curves for epoxy reference samples are shown in Fig. 2.9-D. Unlike samples healed using the DCPD/Grubbs' chemistry, samples healed with epoxy exhibit a stick-slip behavior. Upon further investigation of the load-displacement curve in these samples, unstable crack growth is observed at loads and displacements very similar to the virgin specimen. This confirms the hypothesis that crack pinning mechanisms are present and are highly driven by the composite architecture. Table 2.2 provides results of all DCB testing.

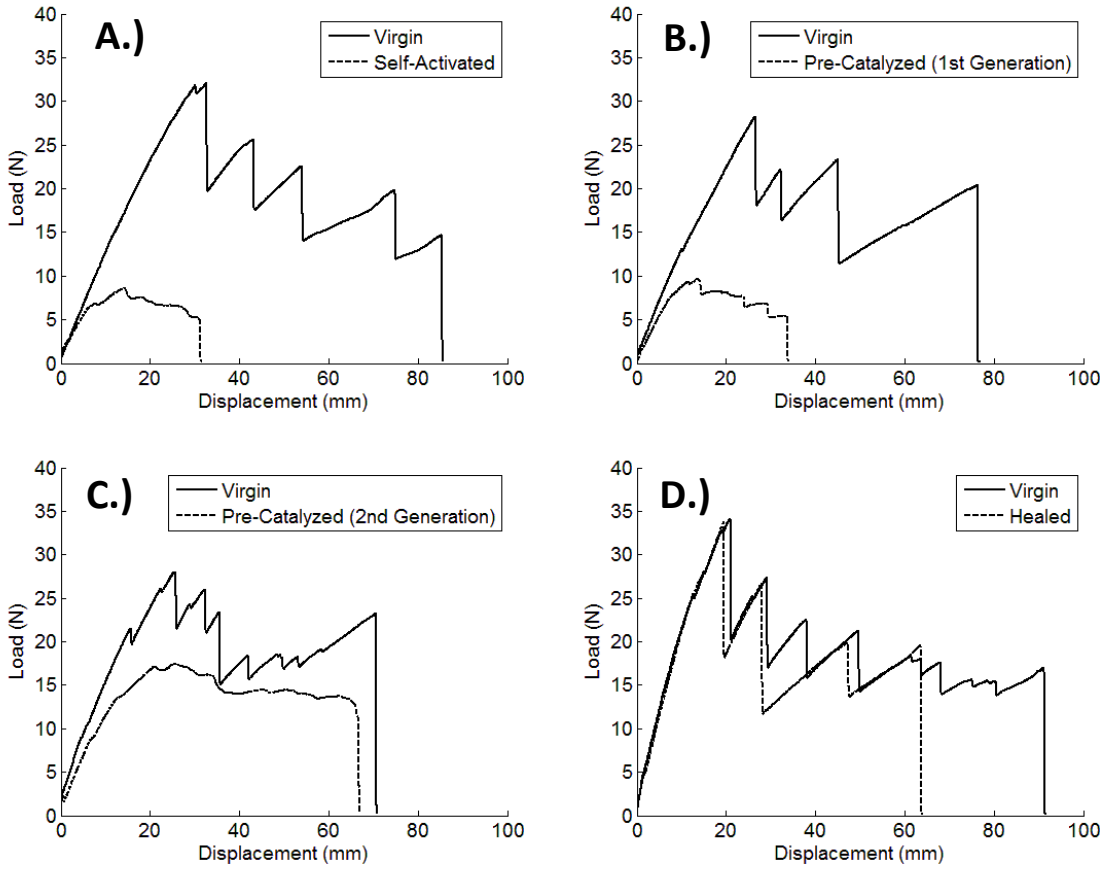

Figure 2.9. Virgin and healed load-displacement curves for self-activated, epoxy reference, second generation pre-catalyzed and first generation pre-catalyzed DCB specimens. Healing agent was injected on to the mid-plane of each sample following virgin testing. Self-activated reference samples contained catalyst functionalized fibers at the sample mid-plane. All other reference samples use plain, un-functionalized fibers. Self-activated specimens (A) use liquid DCPD monomer, first (B) and second (C) generation pre-catalyzed reference samples use a mixture of 1.0 wt% catalyst in DCPD, and epoxy reference samples (D) use Araldite LY / Aradur 8604 as the healing agent.

Fiber Surface	Functionalization	Virgin G_{1C} [J/m2]	Samples	Virgin Fracture Behavior	Reference Test Type	Healing Agent Delivered [μL]	Cure Conditions	# Samples	Healed Fracture Behavior	Healed G_{1C} [J/m2]	Healing Efficiency, η
Plain	None	820 ± 195	15	Stick / Slip	First Generation Pre-catalyzed	200	24 Hours @ 22 °C	3	Stable	110 ± 25	13.4%
					Second Generation Pre-Catalyzed	200	24 Hours @ 22 °C	4	Stable	245 ± 90	29.9%
					Epoxy Reference	200	4 Days @ 22 °C	4	Stick / Slip	715 ± 110	87.2%
					Epoxy Reference	500	4 Days @ 22 °C	4	Stick / Slip	780 ± 285	95.1%
Functionalized	2G Grubbs'	995 ± 135	7	Stick / Slip	Self-Activated	200	24 Hours @ 22 °C	3	Stable	100 ± 30	10.1%
					Self-Activated	500	24 Hours @ 22 °C	4	Stable	85 ± 30	8.5%
	Benzene Only	835 ± 135	7	Stick / Slip	N/A						

Table 2.2. Summary of DCB results.

2.5 Conclusions

Studies have been performed to assess the feasibility of developing a self-healing composite using Grubbs' catalyst functionalized fibers. Woven glass/epoxy composites with functionalized fibers were evaluated using DCB specimens to simulate delamination damage. Pre-catalyzed reference samples demonstrate up to a 30% recovery in critical strain energy release rate, with limited recovery values attributed to poor bonding between polymerized DCPD and glass fibers present on the fracture surface. Pre-catalyzed samples provide a baseline for the optimal healing which can be expected with the Grubbs'/DCPD healing chemistry in this particular system. Second generation pre-catalyzed reference tests demonstrated 3x the healing potential over samples healed with pre-catalyzed first generation healing agents. Self-activated samples showed a 10% recovery of critical strain energy release rate in the best case. The disparity between pre-catalyzed reference samples and self-activated samples arises from catalyst immobility and low catalyst to monomer concentrations in the self-activated samples. Epoxy reference samples demonstrate near full recovery of critical strain energy release rate concluding that limitations of the DCPD/Grubbs' chemistry may be overcome with alternate healing systems.

As a stepping stone towards self-healing of impacted 3D woven glass/epoxy composites, fiber functionalization may provide a pathway to provide catalyst in areas of failure between glass fiber tows during impact damage. However, methods of fiber functionalization and composite manufacture may require optimization to realize the full potential of this method of catalyst delivery in 3D composites.

CHAPTER 3: HIGH TEMPERATURE CURE FIBER-FUNCTIONALIZED COMPOSITES

3.1 Introduction

High performance composite systems often require elevated temperatures for solidification of the matrix material with curing temperatures of 150 °C or more often required. These high temperature cured epoxy systems tend to exhibit increased strength and stiffness over low temperature cure composites and thus are more commonly used in high performance applications. Because of its high thermal stability, second generation Grubbs' catalyst shows promise for applications of self-healing in composites cured at high temperature. In this chapter, extensions of the fiber functionalization technique described in chapter 2 to a high temperature cured glass/epoxy composite are evaluated.

Finding a healing system capable of restoring properties in high temperature cured systems is difficult. One difficulty observed in the original Grubbs'/DCPD healing chemistry is the limited thermal stability of the first generation Grubbs' catalyst. Jones *et al* [29] report deactivation of first generation Grubbs' catalyst at temperatures of 140 °C. This is problematic for high performance composite systems which require temperatures in excess of 150 °C during the curing process. To combat this problem, the second Generation catalyst is selected for high temperature cured systems. Many authors have reported increased thermal stability of the second generation Grubbs' catalyst [27, 28, 33–35] - thus, it is a much more likely to survive the harsh elevated temperatures of high temperature cure composites and is a more suitable candidate for self-healing applications in these materials.

As in chapter 2, double cantilever beam (DCB) specimens are used to evaluate the healing potential. However, in extending the work from chapter 2 to a high temperature cured composite, optimization of the fiber architecture is also explored. Because a high level of interfacial failure is required to expose the surface of the catalyst functionalized fibers, an 8-harness E-glass satin weave is selected for use in this chapter. The nearly unidirectional nature of this fabric makes it suitable to demonstrate increased crack propagation stability and increased interfacial fiber/matrix de-bonding failure mechanisms.

To evaluate this catalyst as a potential for use in high temperature systems, small-scale model double cantilever beam (DCB) specimens are evaluated. While unable to provide true

quantitative data, these small scale specimens provide a semi-quantitative platform for investigating healing potential of the optimized system. Using these model composites allows for many samples to be made in a short time, thus expediting the optimization process.

3.2 Selection of a High Temperature Cure Epoxy

In this chapter the catalyst functionalization is extended to a high temperature cure system. When selecting a resin system, a few requirements were imposed. First, a minimum cure temperature of 150 °C was required to classify the resin as a high-temperature system. Secondly, the amine curing agents must be compatible with the catalyst, as to not deactivate it.

For these studies, Araldite LY / Aradur 8605 (Huntsman Mfg.) was selected. Since the resin system studied in the previous chapter was 8604, its cousin, 8605 was chosen to minimize changes in the matrix material. The manufacture's recommended cure schedule of this resin is 24 hours at room temperature followed immediately by 2 hours at 121 °C, followed immediately by 3 hours at 177 °C. Since the cure schedule reaches a maximum temperature of 177 °C, it is considered a high temperature cured system.

To test catalyst reactivity with the epoxy system, bullet samples were fabricated. To prepare bullet samples, 20 grams of Araldite LY 8605 was mixed with 7 grams of Aradur 8605 (35 pph) in a small cup and degassed under vacuum for 10 minutes. Then, 5 gram aliquots were isolated in a scintillation vial and either first or second generation as received Grubbs' catalyst (Sigma-Aldrich) was mixed in various wt% with the epoxy matrix and degassed an additional 10 minutes. The catalyst imbued resin was then cast into "bullets" measuring 1.5 cm long x 1.0 cm in diameter. Samples were then exposed to the manufacturer's recommend cure. Following processing, samples were removed from the mold and fractured into two halves across the mid-plane using a razor blade and hammer. Once fractured, distilled Dicyclopentadiene (DCPD) monomer (Acros Organics) was injected onto the fracture surface and the two halves were clamped back together and allowed to heal for 24 hours at room temperature. To evaluate healing efficiency, samples were pulled apart along the cylindrical axis with finger force. A qualitative measure of strength, based on a scale of 0-5 was used to record the strength of the healed bond - a result of 0 indicating no bonding, a result of 5 indicating extremely strong bonding. Results, outlined in table 3.1, indicate that no healing occurs in any sample containing first generation Grubbs' catalyst. This is attributed to the thermal deactivation of the catalyst

during the resin cure cycle, as expected. Second generation catalyst, however, showed significant bonding at higher weight percentages. Therefore, the thermal stability and chemical compatibility of the second generation Grubbs' catalyst in the Araldite LY 8605 / Aradur 8605 epoxy system was verified and this epoxy was chosen for all future high temperature cure studies in this chapter.

Catalyst	Catalyst wt%	Ave. Bond Strength Scale 0-5
1st Generation	0.1	0
	0.5	0
	1	0
	2	0
2nd Generation	0.1	0
	0.5	1
	1	2
	2	3

Table 3.1. Results of high temperature cure bullet testing. Araldite LY / Aradur 8605 was used as the polymer host.

3.3 Preform Selection

When optimizing the fiber architecture, a few things must be considered. First, we aim to select an architecture with a weave fine enough so that stick-slip behavior from crack pinning is minimized. This is dictated by fabric weave and by fabric areal density. A more unidirectional weave minimizes stick-slip behavior since the path of the crack is less tortuous and less likely to be interrupted by fiber tows running perpendicular to the crack direction. Lower areal densities also provide fabrics with fiber tows containing less glass fibers per tow. This reduces the size of the tow and minimizes crimping and undulation effects in the crack propagation region of the DCB specimens. However, the tows must be large enough to deposit an adequate amount of catalyst during the catalyst deposition process, so extremely fine fabric weaves were avoided.

Two fabric architectures were evaluated during this optimization - a plain weave, 7.5 oz/yd^2 E-glass fabric (Fibreglast) and a 9 oz/yd^2 eight harness satin E-glass (Fibreglast). Both of these systems have heritage in previous work by Kessler *et al* [22]. Plain composite DCB

specimens were fabricated using the high temperature Araldite LY / Aradur 8605 resin system to evaluate both of these fabrics for potential use.

Composite panels were fabricated using 248mm x 248mm glass fiber preforms in a wet hand lay-up procedure. All samples contained 16 woven layers of fabric. Plain weave specimens were arranged in a $[0]_{16T}$ arrangement, whereas the 8H satin weave fabric was arranged in a $[0\ 90]_{8T}$ arrangement. The epoxy resin matrix was prepared by mixing Araldite LY 8605 resin with Aradur 8605 curing agent (Huntsman Mfg.) at a ratio of 100:35, respectively. Once mixed, the epoxy was degassed for a minimum of 20 minutes under vacuum before use. Four cups of epoxy were individually mixed, one for every four layers of glass fabric.

Once prepared, the first portion of epoxy resin was poured onto the tooling surface of an aluminum plate. A square rubber mold 254 mm x 254 mm was used to contain excess epoxy. Once the tooling surface was adequately coated, four glass fabric layers were lightly placed on the liquid resin with minimal external pressure applied. After approximately ten minutes, full wetting of the fabric was observed. The process was then repeated for the remaining layers. A 248 mm x 102 mm x 25 µm non-porous release film was placed near the mold edge between layers 8 and 9 to provide a pre-crack region for the DCB specimens. Porous peel ply and bleeder cloth were placed over the lay-up to facilitate resin flow in the transverse direction during the curing process. Composites were cured according to table 3.2. Plain weave specimens and 8H satin weave specimens were all approximately 4.0 mm thick. Plain weave specimens and 8H satin weave specimens had a fiber volume fraction of 47% and 48% respectively, calculated by matrix burn-off.

Time, hours	Temperature, °C (°F)	Pressure, kPa
24	22 (70)	172
2	121 (250)	0
3	177 (350)	0

Table 3.2. Cure schedule of DCB specimens fabricated with Araldite LY / Aradur 8605 epoxy.

Following composite manufacture, DCB specimens were cut to size according to ASTM D5528 using a water-jet cooled diamond saw. The crack propagation region of the plain weave specimens was approximately 60 mm whereas the crack propagation region of the 8H satin

weave specimens was approximately 100 mm. The increased crack propagation distance of the 8H satin specimens was provided for verification of an experimental method to be published at another time. This increased crack propagation distance falls into dimension specifications of ASTM D5528 and is in no way believed to significantly affect the results of testing. Piano hinges with a leaf height of 25 mm and an opening distance of 25 mm (National Mfg.) were bonded to the samples using 3M DP-460 High Strength Epoxy. One sample edge was coated with a thin layer of white opaque fluid to aid in visualization of the crack tip during testing. Vertical demarcations were placed along the whitewashed sample edge in 5 mm increments using a fine tip marker to provide a reference for crack length measurements. Demarcations emanated from the end of the pre-crack region and were repeated along the entire crack propagation length.

Specimens were tested on a Parker 081-6079 load frame with a Futek LSB300 50 lb. load cell in displacement control at a rate of 5 mm min^{-1} according to ASTM D5528 [30]. A Basler A631fc CCD camera with an affixed Kowa LM16HC zoom lens was mounted on an optical table beside the sample during testing to track the crack during testing. Load and displacement data was taken at a frequency of 100 Hz and images were recorded at every 200 data points (0.5 Hz). Images were synced with load/displacement data using LABVIEW software. All samples were tested to complete failure. Critical strain energy release rates were calculated using modified beam theory as described in section 2.3.2.

Results of testing are provided in table 3.3. R-curves for the two tests show that while 8H satin weave specimens exhibit a lower critical strain energy release rate, the behavior is much more consistent than the plain weave specimens (Fig. 3.1, Fig. 3.2). Additionally the 8H satin weave specimens exhibit an increase in critical strain energy release rates when the tests begin until a plateau value is reached after approximately 10 mm of crack propagation. The reason for this behavior is the fiber bridging that occurs between the plies during testing, observed in the images taken during the tests (Fig. 3.3). It is hypothesized that this additional fiber exposure will aid in catalyst exposure for samples functionalized with catalyst. Examination of the fracture surface shows increased interfacial fiber/matrix de-bond present in the 8H satin weave specimens as well which will aid in catalyst delivery (Fig. 3.4). Because of the stable fracture behavior and increased fiber exposure from fiber bridging mechanisms, the 8-

harness satin weave fabric was selected for use in the high temperature cure fiber functionalized composite study.

Fabric Weave	Aeral Density [oz/yd2]	Critical Strain Energy Release Rate [J/m2]	# Samples
8H Satin	9	473 ± 23	8
Plain	7.5	1130 ± 145	6

Table 3.3. Results of plain DCB testing

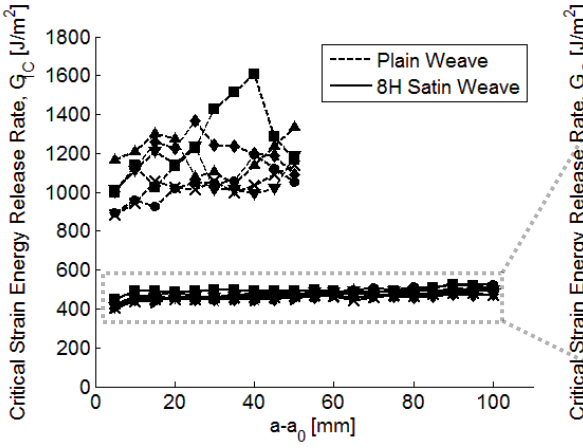

Figure 3.1. R-Curves of plain and 8H satin weave DCB specimens.

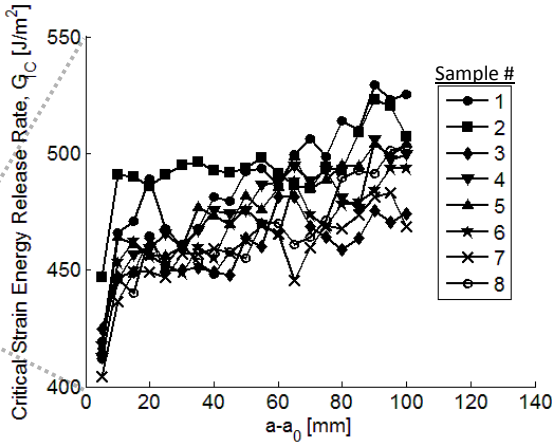

Figure 3.2. R-Curves of 8H satin weave DCB specimens.

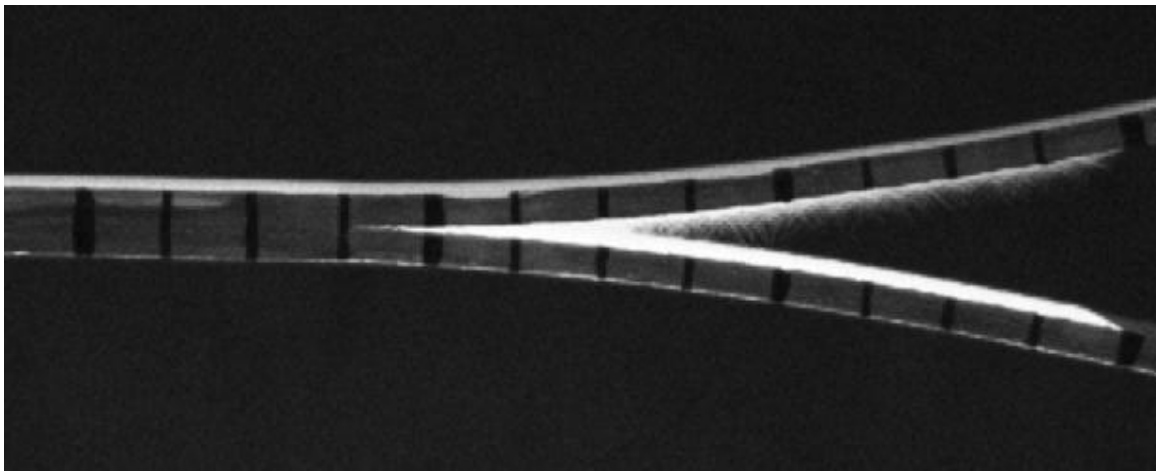

Figure 3.3. Plain 8H Satin Weave DCB Specimen during a mode I fracture test. Fibers protruding from the bulk of the sample into the crack plane indicate the presence of fiber bridging mechanisms.

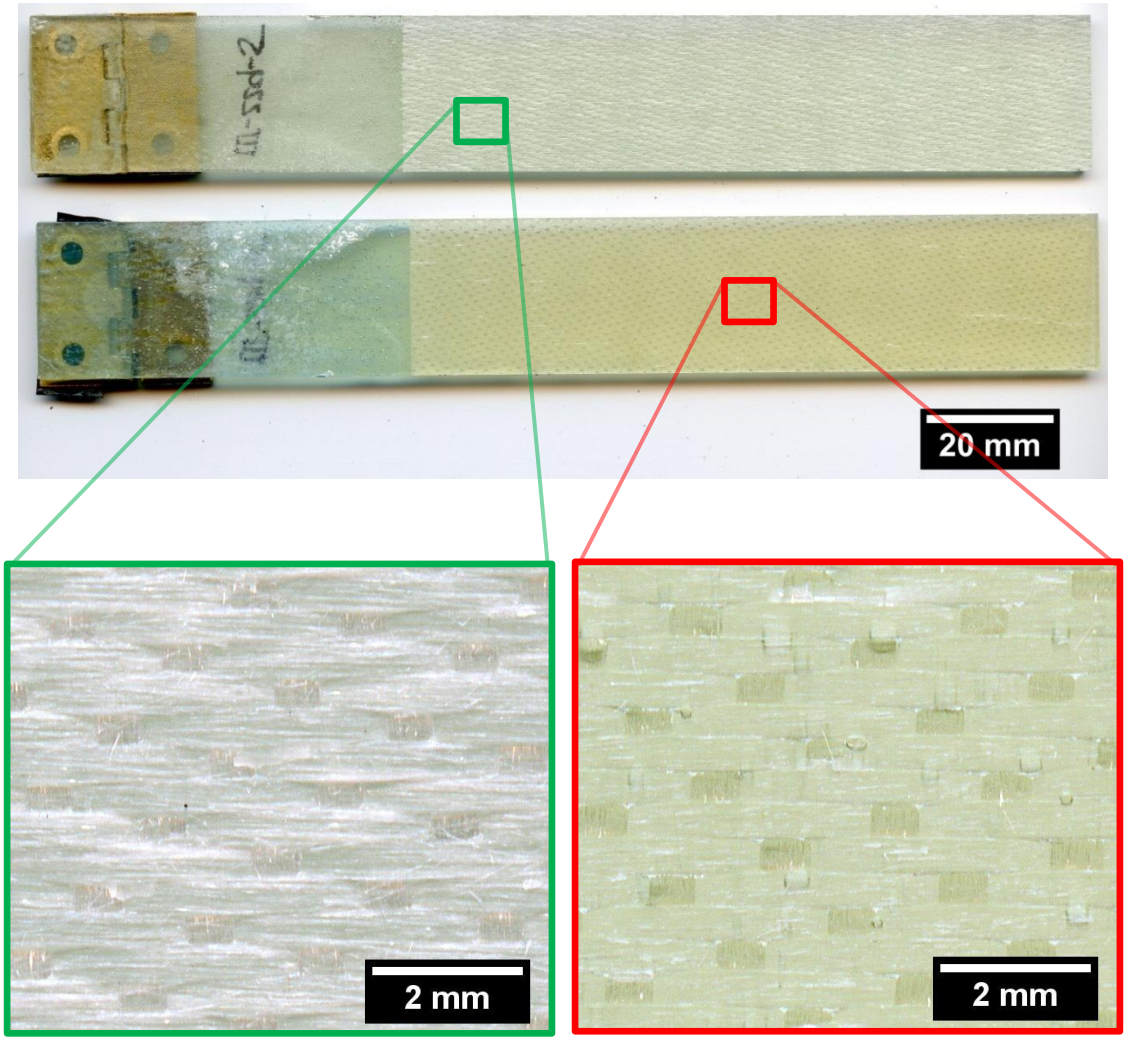

Figure 3.4. Fracture surface of an 8H satin weave specimen following a mode I DCB test. Halves are segregated into resin-rich and resin-lean surfaces indicating significant interfacial fiber/matrix failure.

3.4 Fiber Functionalization

Fiber functionalization becomes a critical factor in the incorporation of catalyst. It dictates the quantity, as well as the dispersion uniformity on the fabric. Two methods of catalyst deposition were evaluated: evaporative crystallization and dip coating. These methods were evaluated to determine how much catalyst could be deposited on the fiber surface and how well the catalyst could be uniformly dispersed.

Both methods utilize a solution of catalyst dissolved in benzene for deposition. To prepare the functionalization solution in both methods, first, gaseous nitrogen was bubbled through benzene (Alfa-Aesar) to remove excess moisture and impurities. Then, either first or second generation Grubbs' catalyst (Sigma-Aldrich) was added to the solvent at a known concentration. Upon the addition of the catalyst, the solution instantly turned a dark purple (first generation) or light red color (second generation) and no catalyst crystals were observed in solution. The solution was allowed to mix for a minimum of 5 minutes on a mixing plate before use. In all cases, no catalyst crystals were observed in solution before use, indicating full dissolution. To evaluate each method, small 25 mm x 100 mm, 9 oz/yd^2, 8H satin weave preforms were used.

In the evaporative crystallization method, fiber preforms were placed in a level crystalizing dish before the catalyst/benzene solution was added. After addition of the solution, the benzene was allowed to evaporate for at least 12 hours creating a super-saturated solution of catalyst in the solvent causing the catalyst to crash out of solution and recrystallize on the surface of the glass fibers. Two concentrations of functionalization solution were used to evaluate the evaporative crystallization method; 0.5 wt% and 3 wt%. In the dip coating method, preforms are dipped into a functionalization solution for approximately ten seconds and then removed. Upon removal, the fabric is held vertically with warp tows pointing downwards for approximately 2 minutes to allow benzene evaporation. In dip coating studies, 3.0 wt% and 10 wt% functionalization solutions were used.

Catalyst deposition using the evaporative crystallization technique is difficult to control. Preforms functionalized with the 0.5 wt% solution exhibited a non-uniform dispersion of the catalyst on the fabric surface. This is most likely due to catalyst migration during the final moments of solvent evaporation. Preforms functionalized with the 3.0 wt% solution had more uniform catalyst dispersion, but exhibited enormous mass changes - up to 43%. In addition, preforms from both evaporative crystallization experiments only contained catalyst on one side of the fabric after functionalization, which is undesirable in a full scale composite system.

Dip coated fabrics offer more consistent coverage and more consistent mass changes. Uniform coverage was optically observed for fabrics coated using either the 3.0 wt% or the 10 wt%. Another benefit of this technique is the speed and scalability. Dip coating is a relatively

quick process, which each dipping process only lasting 10 seconds. Also, it is hypothesized that catalyst coverage on the fibers can be increased simply by increasing the concentration of catalyst in the dip coating solution. This scalability will offer a great advantage when moving to the full scale composite system. Additionally, the catalyst is deposited on both sides of the fabric using this method. Therefore, because of the more uniform coverage, consistent mass changes, and potential scalability of the dip coating method, this method was selected for catalyst deposition on functionalized glass fibers. Images and approximate mass changes of second generation functionalized preforms are provided in table 3.4. These images are representative of first generation catalyst functionalized preforms as well.

Functionalization Technique	Catalyst in Solution, Wt%	Representative Fabric Image	Zoomed Image	Mass Change, Δm
Dip Coating	3.0		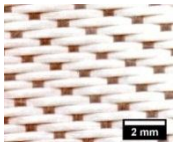	2.09% ± 0.21%
Dip Coating	10.0		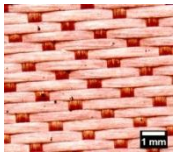	7.34% ± 0.35%
Evaporative Crystallization	1.0		N/A	6.62% ± 1.81%
Evaporative Crystallization	3.0		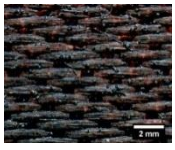	42.40% ± 1.78%

Table 3.4. Second generation catalyst fiber functionalized preforms.

3.5 Model DCBs

To quickly evaluate the potential of these healing systems, small scale model DCB specimens were fabricated. These specimens offer a quick way to qualitatively evaluate the potential

healing of a fiber functionalized composite with a minimal amount of material. Preforms used in the dip coating studies that showed promise for healing were fabricated into model DCBs

Composite model DCB specimens were fabricated using 16 layers of 25 mm x 101 mm, 9 oz/yd^2, 8H satin weave preforms in a $[0\ 90]_{8T}$ layup. Both low temperature (Araldite LY / Aradur 8604) and high temperature (Araldite LY / Aradur 8605) epoxy resin systems were evaluated. The epoxy resin matrix was prepared by mixing either Araldite LY 8605 resin with Aradur 8605 curing agent (Huntsman Mfg.) at a ratio of 100:35, respectively, or by mixing Araldite LY 8604 with Aradur 8604 curing agent at a ratio of 100:15, respectively. Once mixed, the epoxy was degassed for a minimum of 20 minutes under vacuum before use. Four cups of epoxy were individually mixed, one for every four layers of glass fabric.

A rubber mold 305 x 305 x 6.35 mm thick containing ten, 30 mm x 110 mm cut-outs was placed on a Teflon backed aluminum plate and used to prepare individual model DCB specimens. For each 4 layers of fabric in the specimen, approximately 4 grams of epoxy was poured into the mold cavity and given 1 minute to settle. Then four layers of fabric were placed on the resin and given ten minutes to descend into the resin and wet-out. This process was repeated until all 16 layers were placed. In composites tested for self-healing potential, fiber functionalized preforms were placed in layers 8 and 9, with a 25 mm x 50 mm x 23 µm release film placed near the mold edge between them to serve as a pre-crack in the DCB testing. Porous peel ply and bleeder cloth were placed over the lay-up to facilitate resin flow in the transverse direction during the curing process. Specimens were placed in a press to cure. High temperature model DCBs using Araldite LY / Aradur 8605 were cured according to table 3.2. Low temperature model DCBs using Araldite LY / Aradur 8604 were cured for a minimum of 24 hours at room temperature.

Upon removal from the mold, composites were cut using a water-cooled diamond saw to dimensions of approximately 20 mm x 85 mm x 4 mm. End tabs were bonded on and tests were conducted in a manner similar to the method outlined in section 3.4, however in this case, the crack length was not tracked during testing. Displacement and load of each sample was recorded during the virgin tests. Following the virgin tests, 50 µL of distilled DCPD monomer was injected onto the sample crack plane using a microliter syringe. Samples were clamped together using binder clips and allowed a minimum of 24 hours to heal at room temperature.

Samples were then re-tested to evaluate healing potential. Since crack length during these tests was not tracked, quantitative assessments of critical strain energy release rates are not available, however, since the healed and virgin fracture regions emanate from the same location, assessments of energy recovery can be inferred from the load-displacement curves.

3.5.1 Low Temperature Cure Model DCBs

Low temperature cure model DCBs were fabricated to verify the use of the new fabric architecture and verify the new dip coating technique. Results of low temperature cure model DCB testing are outlined in table 3.5.

Resin	Catalyst Deposition Technique	Catalyst	Δm of functionalized fabrics	Healing conditions	Healing	Reference Figure
8604	Dip Coat	2G	2%	RT 24h	None	
8604	Evap Crystallization	2G	40%	RT 24h	High	3.5-A
8604	Dip Coat	1G	9%	RT 24h	High	3.5-B
8604	Dip Coat	1G	9%	80C 24h	Med	3.5-C
8604	Dip Coat	2G	7%	RT 24h	None	
8604	Dip Coat	2G	7%	80C 24h	Low	3.5-D

Table 3.5. Low temperature cure model DCB specimen summary.

Results are variable, but indicate that high levels of healing are possible. Samples functionalized with first generation catalyst show higher potential for recovery in these model specimens. The addition of heat during the cure cycle for first generation catalyst functionalized samples seems to decrease the healing potential, likely due to minor levels of catalyst deactivation at the higher temperatures. The addition of heat in the case of samples functionalized with second generation catalyst aids healing. In general, however, samples functionalized with the second generation catalyst show less potential for healing in the samples tested above.

While most samples tested used preforms that were functionalized by the dip coating method, one sample was tested in which the fiber was functionalized using the evaporative crystallization method. This sample used second generation Grubbs' catalyst and saw a significant level of healing demonstrating that if catalyst loading is high enough, significant recovery is possible.

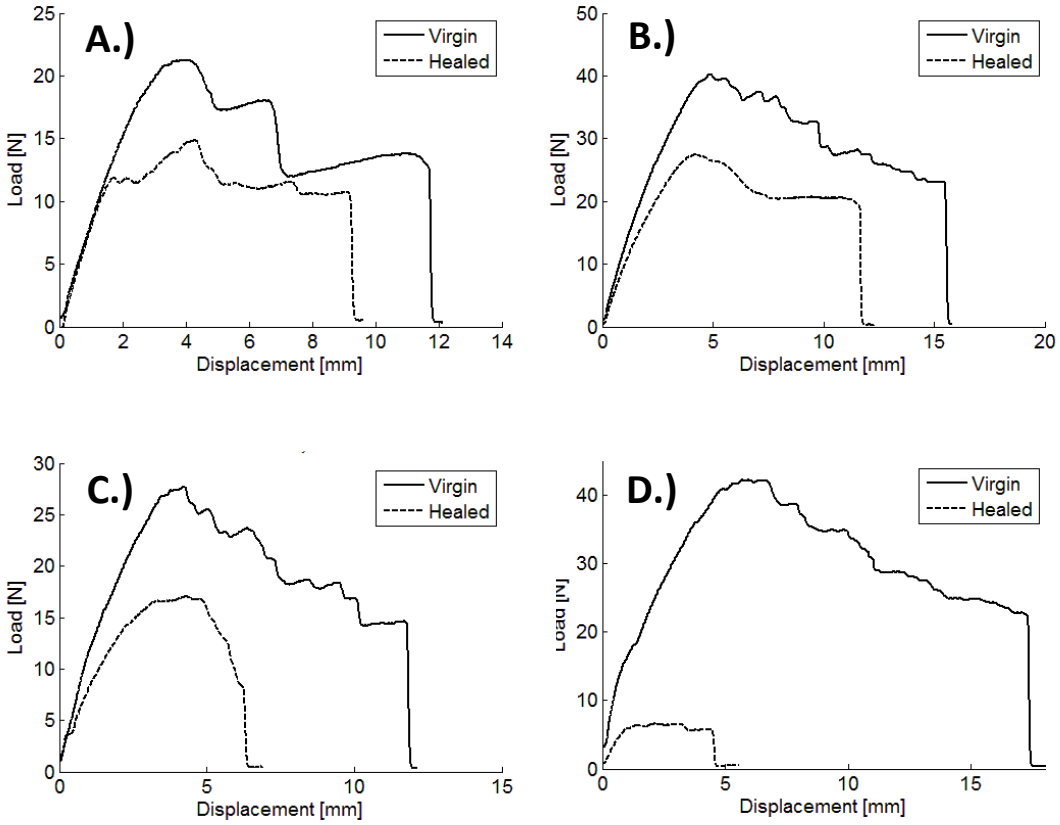

Figure 3.5. Representative load-displacement curves for low temperature cure model DCB specimens. Figure references can be found in table 3.5.

3.5.2 High Temperature Cure Model DCBs

Results of high temperature cure model DCB testing is provided in table 3.6. No healing was observed for any sample that used second generation catalyst functionalized preforms. Oddly enough, the only healing was observed in samples using first generation catalyst in samples that were healed at elevated temperatures. While this seems to conflict with the results of bullet testing from section 3.2, the morphology of the catalyst on the functionalized fiber preforms might offer an increased resistance to deactivation during the high temperature cure cycle.

Resin	Catalyst Deposition Technique	Catalyst	Δm of functionalized fabrics	Healing Conditions	Healing	Reference Figure
8605	Dip Coat	1G	2%	RT 24h	None	
8605	Dip Coat	2G	2%	RT 24h	None	
8605	Dip Coat	1G	9%	RT 24h	None	
8605	Dip Coat	1G	9%	80C 24h	Low	3.6
8605	Dip Coat	2G	7%	RT 24h	None	
8605	Dip Coat	2G	7%	80C 24h	None	

Table 3.6. High temperature cure model DCB specimen summary.

Two hypothesies are offered to explain the lack of healing in the high temperature cure model DCB composites. First, the catalyst exposure in the crack plane may not be high enough. This may occur from lack of catalyst present on the fibers, a lack of fiber exposure during the virgin fracture testing or may occur from catalyst migration from the fracture plane during composite manufacture. Since healing is observed with similar catalyst loading in the low temperature cure system, lack of catalyst present on the fibers is not believed to be the driving factor for limited healing. Minimal fiber exposure is also not believed to be the problem, since virgin fracture testing of plain specimens shows a significant amount of fiber bridinging. Functionalized DCB specimens also show a high level of fiber exposure after testing, as indicated in figure 3.7. The problem may be catalyst migration from the surface of the fibers. Since a large amount of interfacial fiber failure occurs in these tests, migration from the fiber surface into the surrounding resin may significantly limit the catalyst exposure and ultimately, the healing potential. Future work will focus on investigating catalyst migration during composite fabrication.

Lack of catalyst in the crack plane may be a driving factor for limited healing, but catalyst morphology on the surface of the fibers may also cause a problem. Jones *et al* [29] report that catalyst morphology significantly affects cure kinetics of ROMP reactions with Grubbs' catalyst and DCPD. Since fiber functionalization causes the catalyst to crash out and crystallize on the surface of the glass fiber preforms, morphology of the catalyst may be significantly altered. This change in morphology may cause higher surface area to volume ratios of the catalyst, and may increase the potential for catalyst deactivation from thermal and chemical effects. Future work on catalyst morphology must be investigated to determine the full effects of catalyst activity after functionalization.

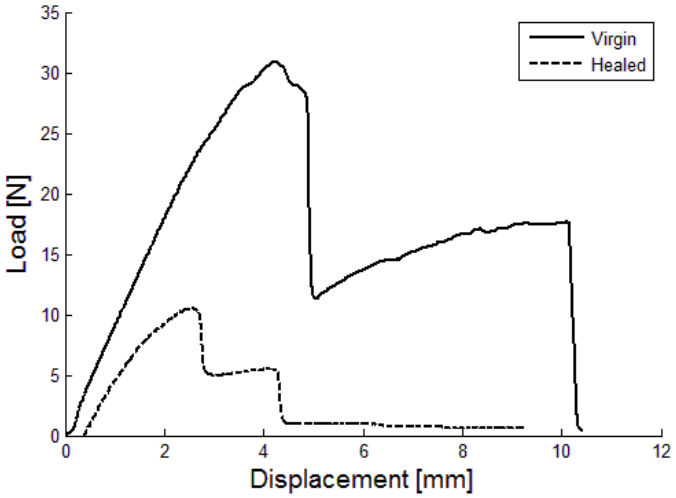

Figure 3.6. Representative load-displacement curve of high temperature cured model DCB specimen. Reference can be found in table 3.6.

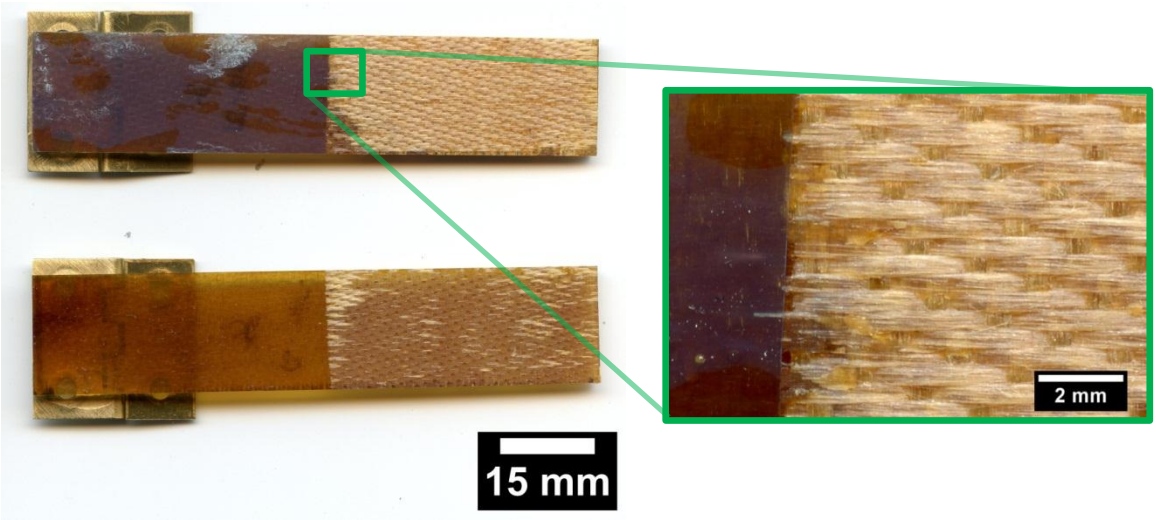

Figure 3.7. Representative fracture surfaces of an 8H satin weave model DCB specimen cured at high temperature with fiber functionalized fabrics at the sample mid-plane. Resin rich and resin lean halves indicate that a high level of fiber/matrix interfacial failure is present.

3.6 Conclusions

In this chapter, catalyst fiber functionalization was examined for potential use in high temperature cure glass/epoxy composites. Small fiber-reinforced composite double cantilever beam specimens made with fiber functionalized preforms qualitatively demonstrate that recovery in high temperature cure composites is possible. Comparisons with low temperature cure composites indicate that catalyst reactivity is decreased when a high temperature cure matrix material is used.

Araldite LY / Aradur 8605 was chosen as a high temperature cure matrix material. The compatibility of first and second generation Grubbs' catalyst was evaluated in this resin system using small polymer bullet samples. First generation catalyst did not retain activity as a ROMP catalyst, as it deactivates during the high temperature cure cycle. However, second generation catalyst retained functionality as a ROMP catalyst and was chosen as a potential candidate for use in a high temperature cure self-healing fiber functionalized glass/epoxy composite.

An 8-harness satin weave fabric was chosen for use as a tool to evaluate fiber functionalization. Double cantilever beam specimens fabricated with this fabric demonstrated more stable crack propagation and increased fiber bridging mechanisms during testing of plain, unfunctionalized samples. Increased fiber bridging mechanisms are required to expose the catalyst during healing cycles after the introduction of mode I interlaminar damage incurred during DCB testing.

Evaluations of catalyst functionalization techniques demonstrated that dip coating methods provided more consistent catalyst coverage on the glass fiber preforms when compared to evaporative crystallization methods. Additionally, the dip coating process is streamlined and catalyst deposition using this method can be achieved quickly.

Small scale model DCB specimens demonstrate healing potential in self-activated tests using both high temperature cure and low temperature cure composites. While high levels of healing were observed for both catalyst types in the low temperature cured composites, minimal healing was observed in the high temperature cured system. Minimal healing is attributed to catalyst migration during composite cure, and coupling affects from increased temperature during cure and increased potential for catalyst deactivation arising from changes in catalyst morphology following the catalyst functionalization process.

Future work investigating the role of catalyst functionalization on the surface of the fibers, as well as catalyst migration during composite manufacture should be explored. Steps must also be taken to incorporate DCPD microcapsules for the evaluation of a fully autonomic healing system.

CHAPTER 4: CONCLUSIONS AND FUTURE WORK

4.1 Conclusions

In this work, fiber functionalization was investigated as a vehicle for incorporating second generation Grubbs' catalyst into a polymer matrix composite for self-healing functionality. In early work, self-activated double cantilever beam (DCB) specimens of 2D woven fiber functionalized composites were used as a test bed to evaluate this method. While recovery of mode I critical strain energy release rate was observed using a low temperature cure glass/epoxy composite, recovery was minor because of complications arising from the coarse fiber architecture. Additionally, the increased thermal stability benefits of the second generation catalyst were not fully realized in a low temperature cure composite. Later work focused on optimization of composite architecture and catalyst deposition techniques to fully realize the potential of the second generation catalyst as a healing agent in high temperature cure composites.

In chapter 2, fiber functionalization was carried out on coarse 24 oz/yd^2, S2-glass plain weave preforms. Preforms were functionalized with second generation Grubbs' catalyst using an evaporative crystallization method. Preforms were then used to make woven composite DCB specimens with a low temperature cure Araldite LY / Aradur 8604 epoxy matrix. Delamination damage incurred during virgin tests of fiber functionalized DCB specimens was healed using liquid DCPD monomer injected onto the specimen fracture surface. Results of this testing demonstrated approximately 10% recovery of critical strain energy release rate. Reference samples using pre-mixed catalyst and monomer demonstrate maximum recovery of 13% and 30% for DCPD polymerization initiated by first and second generation catalyst types, respectively. These results indicate that limited recovery is attributed, in part, to high virgin critical strain energy release rate values occurring from crack pinning mechanisms in virgin samples which cannot be recovered using the Grubbs'/DCPD healing chemistry.

Optimization of fiber architecture and the use of catalyst fiber functionalization in high temperature cure epoxy systems were evaluated in chapter 3. Bullet samples of first and second generation Grubbs' catalyst in high temperature cured Araldite LY / Aradur 8605 showed that the second generation catalyst can survive the high temperature cure process and continue to initiate ROMP, while the first generation catalyst deactivates and loses its potential as a

ROMP catalyst. Optimization of fiber architecture pointed to the use of a 9 oz/yd^2 E-glass 8H satin weave. DCB testing demonstrated increased fiber bridging and more stable crack propagation of this fabric architecture over plain weave architectures of similar areal density. It is hypothesized that increased fiber bridging will increase catalyst exposure in fiber functionalized composites, thus increasing healing potential. Scalable dip coating techniques were investigated as an alternative to evaporative crystallization methods for the deposition of catalyst and found to provide more consistent catalyst coverage on the preforms. Small scale model DCB specimens were used to semi-quantitatively evaluate the required amount of catalyst deposition required to initiate ROMP in these specimens.

4.2 Future Work

While much of this thesis focuses on 2D woven architectures, they are mainly used as a test bed to evaluate fiber functionalization as a use in 3D woven composites. Work done in this thesis demonstrates great potential for the use of fiber functionalization to aid in healing of impact damage in 3D woven preforms using a two part catalyst delivery in which one catalyst is sequestered in wax microspheres to polymerize DCPD in resin-rich areas of the damaged composite and the second catalyst is functionalized on fiber tows to polymerize DCPD monomer in areas of delamination damage between tows. Future work focused on this hybrid healing approach will be carried out using the flexure after impact protocol described by Patel *et al* [21].

Despite the potential of this hybrid systems, inherent limitations exist in the microencapsulated DCPD/Grubbs' healing chemistry first proposed by White *et al* [1] as a use in recovering mechanical properties of 3D orthogonal woven composites subject to out-of-plane impact damage. Even with the advent of catalyst functionalized fibers described in the previous chapters, it is hypothesized that limitations of available monomer volume and weak adhesive bonding between pDCPD and the surrounding materials will ultimately limit healing. Two other healing systems are proposed here in future work for further investigation to overcome the limitations of the Grubbs'/DCPD healing chemistry – an epoxy/amine microencapsulated healing system and an epoxy/amine microvascular based healing system.

4.2.1 Epoxy / Amine Microcapsules

Many authors have reported limited self-healing capability in glass/epoxy composite systems with the Grubbs'/DCPD healing chemistry [3, 22–25]. Single lap shear tests performed by Patel *et al* [21] show that adhesive bonding strength between epoxy substrates using polymerized DCPD is approximately one magnitude of order lower than strength obtained when an epoxy adhesive is utilized. This indicates that an epoxy based healing chemistry has a much higher potential for healing in damaged composite systems. This higher healing potential has been partially realized by Trask *et al* [36] in microvascular composite systems, however, studies by these authors have consistently used manually delivered, pre-mixed liquid epoxy, so a fully autonomic self-healing composite system has yet to be demonstrated.

Recent advancements in microencapsulation techniques by Jin *et al* [37], however, have allowed for the encapsulation of epoxy and amine chemistries for fully autonomic self-healing systems. Authors of this work describe a process in which diluted epoxy monomer and liquid aliphatic polyamine cross-linking agents are each individually sequestered in separate microcapsules for self-healing applications. Self-healing results in this work demonstrated up to 90% healing efficiencies in bulk polymer systems. This system should be explored as an alternative method for self-healing in composites subject to impact damage because of the increased healing potential available with the epoxy/amine chemistry.

4.2.2 Microvascular Composites

While the microencapsulated epoxy/amine based healing system shows promise, it still suffers from the short-comings of all microencapsulated self-healing systems, namely, limitations of available healing agent and limited capability of healing damage multiple times in a single area. The connectivity of microvascular systems, however, offers a way to combat these shortcomings.

Healing of large damage volumes in microvascular composites has been demonstrated by many authors. Bond and coworkers have investigated the use of hollow glass fibers (HGFs) for use as a microvascular based healing system. HGFs were filled with various fluids using a vacuum infiltration technique. Original work used 15 μm diameter fibers, but healing was minimal because of a limited delivery of healing components [38]. Later work used larger, 60 μm diameter HGFs. Studies were done to investigate the effects of sequestering the two part

healing chemistry in separate channels [39–42] or premixing the components before infiltration [41, 43, 44]. Sandwich panels with internal microvascular networks have been studied by Williams *et al* [45]. Each of these studies demonstrated recovery of properties in composite structures with relatively large damage volumes.

Additionally, microvascular based healing systems have been used to achieve multiple healing cycles in a variety of materials. Toohey *et al* [46, 47] used 3D vascular networks fabricated through direct write-assembly techniques to heal brittle coatings on the surface of a bulk polymer using the original DCPD/Grubbs' healing chemistry. Up to 16 healing cycles were achieved in this work. Hansen *et al* [48, 49] extended self-healing coating process to epoxy based healing systems using a similar direct write assembly process enabling up to 30 healing cycles. Hamilton *et al* [50] explored the use of microvascular networks to achieve up to 13 healing cycles in a bulk polymer.

New developments in microvascular network fabrication in polymer composite systems give rise to exploration of more complex network architectures for self-healing of impact damage in woven composite systems. Esser-Kahn *et al* [51] and Dong *et al* [52] have investigated the use of a chemically treated poly(lactic acid) fiber for the manufacture of more complex 3D networks in composite materials. In this work, PLA fibers are first woven into a composite preform before matrix infusion and solidification. Following the composite cure, fibers are evacuated via de-polymerization and vaporization of monomeric byproducts leaving an internal vasculature in the composite which inversely replicates the original PLA fiber network. Fibers diameters of between 20 μm and 500 μm at lengths up to 1 m have been successfully removed from epoxy specimens. Another advancement in 3D microvascular network design has been explored by Huang *et al* [53] using the dielectric breakdown properties of polymers to create highly branched tree-like microchannels. Both of these advancements provide a significant step forward in the design of internal microvascular networks for use in self-healing polymers and composites.

REFERENCES

[1] S. R. White, N. R. Sottos, P. H. Geubelle, J. S. Moore, M. R. Kessler, S. R. Sriram, E. N. Brown, and S. Viswanathan, "Autonomic healing of polymer composites," *Nature*, vol. 409, no. 6822, pp. 794–797, Feb. 2001.

[2] B. J. Blaiszik, S. L. B. Kramer, S. C. Olugebefola, J. S. Moore, N. R. Sottos, and S. R. White, "Self-Healing Polymers and Composites," *Annual Review of Materials Research*, vol. 40, no. 1, pp. 179–211, Jun. 2010.

[3] A. J. Patel, N. R. Sottos, E. D. Wetzel, and S. R. White, "Autonomic healing of low-velocity impact damage in fiber-reinforced composites," *Composites Part A: Applied Science and Manufacturing*, vol. 41, no. 3, pp. 360–368, Mar. 2010.

[4] R. A. Chaudhuri, M. Xie, and H. J. Garala, "Stress Singularity Due to Kink Band Weakening a Unidirectional Composite Under Compression," *Journal of Composite Materials*, vol. 30, no. 6, pp. 672–691, Apr. 1996.

[5] S. Sivashanker, N. A. Fleck, and M. P. F. Sutcliffe, "Microbuckle propagation in a unidirectional carbon fibre-epoxy matrix composite," *Acta Materialia*, vol. 44, no. 7, pp. 2581–2590, Jul. 1996.

[6] P. Berbinau, C. Soutis, and I. A. Guz, "Compressive failure of 0° unidirectional carbon-fibre-reinforced plastic (CFRP) laminates by fibre microbuckling," *Composites Science and Technology*, vol. 59, no. 9, pp. 1451–1455, Jul. 1999.

[7] T. V. Parry and A. S. Wronski, "Kinking and compressive failure in uniaxially aligned carbon fibre composite tested under superposed hydrostatic pressure," *Journal of Materials Science*, vol. 17, no. 3, pp. 893–900, 1982.

[8] M. H. Mohamed and A. K. Bilisik, "Multi-layer three-dimensional fabric and method for producing," U.S. Patent 546576014-Nov-1995.

[9] S. L. Gao and J. K. Kim, "Three-Dimensional Characterization of Impact Damage in CFRPs," *Key Engineering Materials*, vol. 141–143, pp. 35–54, 1998.

[10] J.-K. Kim and M.-L. Sham, "Impact and delamination failure of woven-fabric composites," *Composites Science and Technology*, vol. 60, no. 5, pp. 745–761, Apr. 2000.

[11] S.-L. Gao and J.-K. Kim, "Scanning acoustic microscopy as a tool for quantitative characterisation of damage in CFRPs," *Composites Science and Technology*, vol. 59, no. 3, pp. 345–354, Feb. 1999.

[12] J.-K. Kim, D. B. MacKay, and Y.-W. Mai, "Drop-weight impact damage tolerance of CFRP with rubber-modified epoxy matrix," *Composites*, vol. 24, no. 6, pp. 485–494, Sep. 1993.

[13] M. D. Rhodes, J. G. Williams, and J. H. Starnes Jr., "Low-velocity impact damage in graphite-fiber reinforced epoxy laminates," *Polymer Composites*, vol. 2, no. 1, pp. 36–44, Jan. 1981.

[14] G. J. Williams, I. P. Bond, and R. S. Trask, "Compression after impact assessment of self-healing CFRP," *Composites Part A: Applied Science and Manufacturing*, vol. 40, no. 9, pp. 1399–1406, Sep. 2009.

[15] G. P. McCombe, J. Rouse, R. S. Trask, P. J. Withers, and I. P. Bond, "X-ray damage characterisation in self-healing fibre reinforced polymers," *Composites Part A: Applied Science and Manufacturing*, vol. 43, no. 4, pp. 613–620, Apr. 2012.

[16] C. S. Lopes, O. Seresta, Y. Coquet, Z. Gürdal, P. P. Camanho, and B. Thuis, “Low-velocity impact damage on dispersed stacking sequence laminates. Part I: Experiments,” *Composites Science and Technology*, vol. 69, no. 7–8, pp. 926–936, Jun. 2009.
[17] C. S. Lopes, P. P. Camanho, Z. Gürdal, P. Maimí, and E. V. González, “Low-velocity impact damage on dispersed stacking sequence laminates. Part II: Numerical simulations,” *Composites Science and Technology*, vol. 69, no. 7–8, pp. 937–947, Jun. 2009.
[18] J. N. Baucom and M. A. Zikry, “Low-velocity impact damage progression in woven E-glass composite systems,” *Composites Part A: Applied Science and Manufacturing*, vol. 36, no. 5, pp. 658–664, May 2005.
[19] J. N. Baucom, M. A. Zikry, and A. M. Rajendran, “Low-velocity impact damage accumulation in woven S2-glass composite systems,” *Composites Science and Technology*, vol. 66, no. 10, pp. 1229–1238, Aug. 2006.
[20] J. D. Rule, N. R. Sottos, and S. R. White, “Effect of microcapsule size on the performance of self-healing polymers,” *Polymer*, vol. 48, no. 12, pp. 3520–3529, Jun. 2007.
[21] A. Patel, “Autonomic healing of low-velocity impact damage in woven fiber-reinforced composites,” University of Illinois at Urbana-Champaign, United States -- Illinois, 2011.
[22] M. . Kessler and S. . White, “Self-activated healing of delamination damage in woven composites,” *Composites Part A: Applied Science and Manufacturing*, vol. 32, no. 5, pp. 683–699, May 2001.
[23] M. . Kessler, N. . Sottos, and S. . White, “Self-healing structural composite materials,” *Composites Part A: Applied Science and Manufacturing*, vol. 34, no. 8, pp. 743–753, Aug. 2003.
[24] B. J. Blaiszik, M. Baginska, S. R. White, and N. R. Sottos, “Autonomic Recovery of Fiber/Matrix Interfacial Bond Strength in a Model Composite,” *Advanced Functional Materials*, vol. 20, no. 20, pp. 3547–3554, Oct. 2010.
[25] K. Sanada, I. Yasuda, and Y. Shindo, “Transverse tensile strength of unidirectional fibre-reinforced polymers and self-healing of interfacial debonding,” *Plastics, Rubber and Composites*, vol. 35, no. 2, pp. 67–72, Mar. 2006.
[26] E. Brown, N. Sottos, and S. White, “Fracture testing of a self-healing polymer composite,” *Experimental Mechanics*, vol. 42, no. 4, pp. 372–379, 2002.
[27] G. O. Wilson, M. M. Caruso, N. T. Reimer, S. R. White, N. R. Sottos, and J. S. Moore, “Evaluation of Ruthenium Catalysts for Ring-Opening Metathesis Polymerization-Based Self-Healing Applications,” *Chemistry of Materials*, vol. 20, no. 10, pp. 3288–3297, May 2008.
[28] G. O. Wilson, K. A. Porter, H. Weissman, S. R. White, N. R. Sottos, and J. S. Moore, “Stability of Second Generation Grubbs’ Alkylidenes to Primary Amines: Formation of Novel Ruthenium-Amine Complexes,” *Advanced Synthesis & Catalysis*, vol. 351, no. 11–12, pp. 1817–1825, Aug. 2009.
[29] A. S. Jones, J. D. Rule, J. S. Moore, S. R. White, and N. R. Sottos, “Catalyst Morphology and Dissolution Kinetics of Self-Healing Polymers,” *Chem. Mater.*, vol. 18, no. 5, pp. 1312–1317, 2006.
[30] ASTM D5528, “ASTM D5528 - Standard Test Method for Mode I Interlaminar Fracture Toughness of Unidirectional Fiber-Reinforced Polymer Matrix Composites.” .

[31] S. Hashemi, A. J. Kinloch, and J. G. Williams, “Corrections needed in double-cantilever beam tests for assessing the interlaminar failure of fibre-composites,” *Journal of Materials Science Letters*, vol. 8, no. 2, pp. 125–129, 1989.
[32] I. A. Ashcroft, D. J. Hughes, and S. J. Shaw, “Mode I fracture of epoxy bonded composite joints: 1. Quasi-static loading,” *International Journal of Adhesion and Adhesives*, vol. 21, no. 2, pp. 87–99, 2001.
[33] S. B. Garber, J. S. Kingsbury, B. L. Gray, and A. H. Hoveyda, “Efficient and Recyclable Monomeric and Dendritic Ru-Based Metathesis Catalysts,” *J. Am. Chem. Soc.*, vol. 122, no. 34, pp. 8168–8179, 2000.
[34] H. Wakamatsu and S. Blechert, “A Highly Active and Air-Stable Ruthenium Complex for Olefin Metathesis,” *Angewandte Chemie International Edition*, vol. 41, no. 5, pp. 794–796, Mar. 2002.
[35] L. Guadagno, P. Longo, M. Raimondo, C. Naddeo, A. Mariconda, V. Vittoria, G. Iannuzzo, and S. Russo, “Use of Hoveyda–Grubbs’ second generation catalyst in self-healing epoxy mixtures,” *Composites Part B: Engineering*, vol. 42, no. 2, pp. 296–301, Mar. 2011.
[36] R. S. Trask, H. R. Williams, and I. P. Bond, “Self-healing polymer composites: mimicking nature to enhance performance,” *Bioinspiration & Biomimetics*, vol. 2, no. 1, p. P1–P9, Mar. 2007.
[37] H. Jin, C. L. Mangun, D. S. Stradley, J. S. Moore, N. R. Sottos, and S. R. White, “Self-healing thermoset using encapsulated epoxy-amine healing chemistry,” *Polymer*, vol. 53, no. 2, pp. 581–587, Jan. 2012.
[38] S. . Bleay, C. . Loader, V. . Hawyes, L. Humberstone, and P. . Curtis, “A smart repair system for polymer matrix composites,” *Composites Part A: Applied Science and Manufacturing*, vol. 32, no. 12, pp. 1767–1776, Dec. 2001.
[39] J. W. C. Pang and I. P. Bond, “‘Bleeding composites’—damage detection and self-repair using a biomimetic approach,” *Composites Part A: Applied Science and Manufacturing*, vol. 36, no. 2, pp. 183–188, Feb. 2005.
[40] J. W. C. Pang and I. P. Bond, “A hollow fibre reinforced polymer composite encompassing self-healing and enhanced damage visibility,” *Composites Science and Technology*, vol. 65, no. 11–12, pp. 1791–1799, Sep. 2005.
[41] R. S. Trask and I. P. Bond, “Biomimetic self-healing of advanced composite structures using hollow glass fibres,” *Smart Materials and Structures*, vol. 15, no. 3, pp. 704–710, Jun. 2006.
[42] R. S. Trask, G. J. Williams, and I. P. Bond, “Bioinspired Self-Healing of Advanced Composite Structures Using Hollow Glass Fibres,” *J. R. Soc. Interface*, vol. 4, no. 13, pp. 363–371, Apr. 2007.
[43] G. Williams, R. Trask, and I. Bond, “A self-healing carbon fibre reinforced polymer for aerospace applications,” *Composites Part A: Applied Science and Manufacturing*, vol. 38, no. 6, pp. 1525–1532, Jun. 2007.
[44] C. J. Norris, G. J. Meadway, M. J. O’Sullivan, I. P. Bond, and R. S. Trask, “Self-Healing Fibre Reinforced Composites via a Bioinspired Vasculature,” *Advanced Functional Materials*, vol. 21, no. 19, pp. 3624–3633, Oct. 2011.
[45] H. R. Williams, R. S. Trask, and I. P. Bond, “Self-healing sandwich panels: Restoration of compressive strength after impact,” *Composites Science and Technology*, vol. 68, no. 15–16, pp. 3171–3177, Dec. 2008.

[46] K. S. Toohey, C. J. Hansen, J. A. Lewis, S. R. White, and N. R. Sottos, “Delivery of Two-Part Self-Healing Chemistry via Microvascular Networks,” *Advanced Functional Materials*, vol. 19, no. 9, pp. 1399–1405, May 2009.
[47] K. Toohey, N. Sottos, and S. White, “Characterization of Microvascular-Based Self-healing Coatings,” *Experimental Mechanics*, vol. 49, no. 5, pp. 707–717, 2009.
[48] C. J. Hansen, W. Wu, K. S. Toohey, N. R. Sottos, S. R. White, and J. A. Lewis, “Self-Healing Materials with Interpenetrating Microvascular Networks,” *Advanced Materials*, vol. 21, no. 41, pp. 4143–4147, Nov. 2009.
[49] C. J. Hansen, S. R. White, N. R. Sottos, and J. A. Lewis, “Accelerated Self-Healing Via Ternary Interpenetrating Microvascular Networks,” *Advanced Functional Materials*, vol. 21, no. 22, pp. 4320–4326, Nov. 2011.
[50] A. R. Hamilton, N. R. Sottos, and S. R. White, “Self-Healing of Internal Damage in Synthetic Vascular Materials,” *Advanced Materials*, vol. 22, no. 45, pp. 5159–5163, Dec. 2010.
[51] A. P. Esser-Kahn, P. R. Thakre, H. Dong, J. F. Patrick, V. K. Vlasko-Vlasov, N. R. Sottos, J. S. Moore, and S. R. White, “Three-Dimensional Microvascular Fiber-Reinforced Composites,” *Advanced Materials*, vol. 23, no. 32, pp. 3654–3658, Aug. 2011.
[52] H. Dong, A. P. Esser-Kahn, P. R. Thakre, J. F. Patrick, N. R. Sottos, S. R. White, and J. S. Moore, “Chemical Treatment of Poly(lactic acid) Fibers to Enhance the Rate of Thermal Depolymerization,” *ACS Applied Materials & Interfaces*, vol. 4, no. 2, pp. 503–509, Feb. 2012.
[53] J. Huang, J. Kim, N. Agrawal, A. P. Sudarsan, J. E. Maxim, A. Jayaraman, and V. M. Ugaz, “Rapid Fabrication of Bio-inspired 3D Microfluidic Vascular Networks,” *Advanced Materials*, vol. 21, no. 35, pp. 3567–3571, Sep. 2009.